INTERNATIONAL JOURNAL OF CLIMATOLOGY
Int. J. Climatol. (2014)
Published online in Wiley Online Library
(wileyonlinelibrary.com) DOI: 10.1002/joc.4192

Changing temperature and precipitation extremes in the Hindu Kush-Himalayan region: an analysis of CMIP3 and CMIP5 simulations and projections

Prajjwal K. Panday,[a*] Jeanne Thibeault[b] and Karen E. Frey[c]

[a] *The Woods Hole Research Center, Falmouth, MA, USA*
[b] *Department of Geography, University of Connecticut, Storrs, CT, USA*
[c] *Graduate School of Geography, Clark University, Worcester, MA, USA*

ABSTRACT: The Hindu Kush-Himalayan (HKH) region epitomizes a geographic region where cryospheric processes coupled with hydrological regimes are under threat owing to a warming climate and shifts in climate extremes. In this study, we analyse global climate models in the Coupled Model Intercomparison Project phase 3 (CMIP3) and phase 5 (CMIP5) archives to investigate the qualitative aspects of change and trends in temperature and precipitation indices. Specifically, we examine and evaluate multi-model, multi-scenario climate change projections and seven extreme temperature and precipitation indices over the eastern Himalaya (EH) and western Himalaya-Karakoram (WH) regions for the 21st century. Density distribution plots of observed climate indices for meteorological stations and gridded indices are also analysed, which indicate significant negative trends in the annual number of frost days and significant increasing trends in warm nights in the EH region over the 1960–2000 period. Multi-model average (MMA) projections additionally indicate continued trends towards more extreme conditions consistent with a warmer, wetter climate. Precipitation projections indicate increased mean precipitation with more frequent extreme rainfall during monsoon season in the EH region, and a wetter cold season in the WH region. Time series of all MMA precipitation indices exhibit significant increasing trends over the 1901–2099 period. By comparison, time series of temperature indices show decreases in the intra-annual extreme temperature range and total number of frost days, as well as increases in warm nights. In general, these future projections point towards increases in summertime temperatures and modifications in precipitation across both regions.

KEY WORDS CMIP5; CMIP3; climate change; climate extremes; Hindu Kush-Himalaya; climate model; ensemble

Received 2 November 2012; Revised 5 August 2014; Accepted 29 September 2014

1. Introduction

The Hindu Kush-Himalayan (HKH) region lies in the high elevations of central Asia, which has been identified as one of the most sensitive areas susceptible to global climate change (Xu *et al.*, 2009). Despite the importance of this region, there is currently no comprehensive assessment of climate change projections and climate extremes over the HKH. As climate scenarios are increasingly used in impacts research, decision support, and vulnerability assessments (Lobell *et al.*, 2008; Mote *et al.*, 2011), and as future climate projections are expected to use a much more diverse set of model types (Overpeck *et al.*, 2011), an analysis of existing climate data, simulations, and extremes for the HKH region is necessary. The impacts of climate change such as flooding, drought, and weather hazards are typically manifested through changes in extremes (Easterling *et al.*, 2000; Klein Tank *et al.*, 2006; Kharin *et al.*, 2007; Coumou and Rahmstorf, 2012) and, therefore, it is critical to examine the observed and projected future changes in these extremes (Tebaldi *et al.*, 2006). In addition, any impact analysis study will require climate information with regional detail for which dynamical and statistical downscaling techniques are commonly used; however, it is important to evaluate the results of global climate models (GCMs) prior to downscaling since the limitations and uncertainty inherent in climate simulations are inevitably transferred to the regional results (Tebaldi and Knutti, 2010). The use of multi-model ensembles not only provides information about variability among model projections but also provides an opportunity to understand the regional behaviour of climate extremes across models and scenarios.

Flash floods, outburst floods, landslides, hazardous weather, and agricultural threats are usually visible as extremes and are particularly important in mountainous regions (Marengo *et al.*, 2009; Huggel *et al.*, 2010; Thibeault *et al.*, 2010). Flooding in surrounding lowlands can be exacerbated, particularly during summer monsoon months when intense precipitation events are concentrated in upstream highlands of the Himalayan

* Correspondence to: P. K. Panday, Woods Hole Research Center, 149 Woods Hole Road, Falmouth, MA 02540, USA. E-mail: ppanday@whrc.org

region (Sen, 2009). In the highlands, snowmelt runoff generation in regions where winter temperatures are near freezing may be impacted by increasing winter temperatures, thereby leading to shifts from snow-dominated to rainfall-dominated regimes (Nolin and Daly, 2006; Adam *et al.*, 2009). Therefore, there has been a call to strengthen the modelling efforts for climate projections required to close knowledge gaps in understanding high altitude hydrological processes and future projections in rainfall and temperature (Bolch *et al.*, 2012; Rajbhandari *et al.*, 2014).

Availability of multi-model climate simulations performed for the Fourth and Fifth Assessment Reports (AR4 and AR5) of the Intergovernmental Panel on Climate Change (IPCC) provides an opportunity to assess the ability of these models to reproduce historical climate (20th century) and to evaluate the climate change projections for the 21st century. The IPCC AR4 and AR5 model simulations as well as simulated temperature and precipitation extremes are available from the World Climate Research Programme's Coupled Model Intercomparison Project phase 3 (CMIP3) and phase 5 (CMIP5) multi-model data sets (Meehl *et al.*, 2007; Taylor *et al.*, 2012). Tebaldi *et al.* (2006) have analysed historical and future simulations of ten climate extreme indices from the CMIP3 data set and concluded that model simulations of historical trends for both temperature- and precipitation-related extremes agree well with observations at the continental and global scales. Sillmann *et al.* (2013a) have analysed climate extreme indices from the CMIP5 models and reanalysis data, and shown that the models are generally able to simulate climate extremes and their trend patterns when compared with gridded observational indices. HadEX2 data provide a suite of climate extreme indices derived from globally observed temperature and precipitation data and represent various facets of a changing global climate in its intensity, frequency, and duration (Donat *et al.*, 2013). These projections show a trend towards a warmer, wetter global climate with greater precipitation intensity.

There have been numerous other studies utilizing both CMIP3 and CMIP5 data sets and regional climate simulations across various regions (Vera and Silvestri, 2009; Coppola and Giorgi, 2010; Fan *et al.*, 2010; Yang *et al.*, 2012); however, a comprehensive assessment of climate projections for the Himalayan region is lacking. A previous report summarizes the regional climate model scenarios provided by the Hadley Centre Regional Model 2 (HadRM2) and Providing Regional Climates for Impacts Studies (PRECIS) models for the eastern Himalaya (EH) (Shrestha and Devkota, 2010). HadRM2 simulations over the EH region projected a 2.9 °C increase in the annual mean temperature by the 2050s. PRECIS simulations for B2 and A2 scenarios projected a 2.9 and 4.3 °C increase, respectively, in annual mean temperature by the 2080s. HadRM2 simulations of this region projected an increase of 18% of the current precipitation simulations by the 2050s, whereas PRECIS simulations for B2 and A2 scenarios projected increases of annual precipitation by 13 and 34%, respectively, by the 2080s (Shrestha and Devkota, 2010). Other studies have utilized the CMIP3 data set to understand the behaviour of the South Asian summer monsoon and its connection with the El Niño-Southern Oscillation (ENSO) and Eurasian snow cover (Fan *et al.*, 2010; Peings and Douville, 2010). Seth *et al.* (2011) analysed coupled climate model projections of global land monsoons, which show a modification of the annual cycle of tropical precipitation with reductions in spring and increases in summer precipitation. The study identified remote mechanisms (increased tropospheric stability) leading to a spring decrease in precipitation, and local mechanisms (enhanced evapotranspiration and decreased tropospheric stability) leading to increased precipitation during the rainy season. This study focuses on the model intercomparison simulations so as to establish a multi-model baseline for the HKH region.

The HKH region spans a large geographic area and, therefore, consists of varied topography and climate (Figure 1). A recent study analysing long-term satellite measurements (1979–2007) found greater warming rates over the WH region (0.26 ± 0.09 °C decade^{-1}) that significantly exceed the entire HKH as well as overall global warming rates (Gautam *et al.*, 2010). Other factors that exhibit significant variability across the region include: (1) precipitation variability, with monsoonal precipitation dominating EH hydro-climatological patterns and westerly dominated precipitation influencing the WH regions (Young and Hewitt, 1990; Chalise, 1994); (2) glacier characteristics, with the Karakoram consisting of long, interconnected glacial systems as opposed to smaller individual glaciers in the Himalayan range (Williams and Ferrigno, 2010); (3) snowmelt dynamics, with the EH region having an earlier melt onset, later freeze-up, and a longer melt season relative to other regions across the HKH (Panday *et al.*, 2011); and (4) glacier response times, with more melting and faster glacial retreat in the EH but a lack of any rapid disintegration of glaciers in the northwestern Himalaya and Karakoram regions (Kargel *et al.*, 2009; Bolch *et al.*, 2012; Gardelle *et al.*, 2012). Although the global model simulations are of coarse spatial scale (approximately 1–3°), the Himalayan and Karakoram regions are geographically large (with a combined area of approximately 692 000 km^2), which allows for an examination and comparison of climate projections and scenarios between the EH and WH regions.

This study uses CMIP3 and CMIP5 models to examine their ability to represent 20th century climate and analyse the evolution of extreme temperature and precipitation indices into the future for the EH and WH regions using the Special Reports on Emission Scenarios (SRES) B1 (low-range emissions), A1B (mid-range emissions), A2 (high-range emissions), and Representative Concentration Pathway (RCP) 8.5 (high end emissions) scenarios. This study examines seven climate extreme indices computed for both CMIP generation models. Additionally, time evolution of EH and WH area-averaged multi-model ensemble

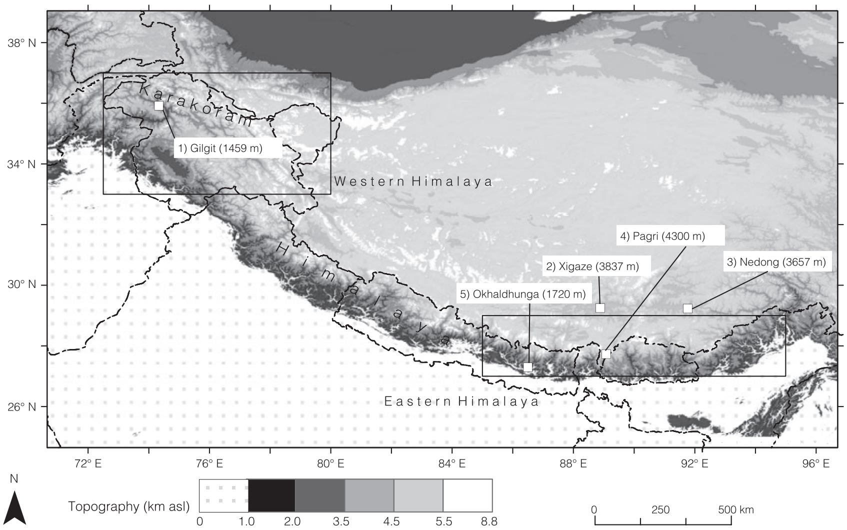

Figure 1. The EH and WH regions showing high altitude stations with long-term meteorological data and extreme climate indices.

extreme indices is examined, along with changes in density distributions for the middle (2020–2049) and the late (2070–2099) 21st century. The EH is defined as spanning an area from 27° to 29°N and 85° to 95°E, whereas the WH is defined by the bounding area spanning 33°–37°N and 72.5°–80°E (Figure 1).

2. Data and methods

2.1. CMIP climate extreme indices

The CMIP3 and CMIP5 models are an effort by the World Climate Research Programme's Working Group on Climate Models where several modelling groups around the world contributed to a coordinated set of 20th and 21st century climate simulations (Meehl *et al.*, 2007; Taylor *et al.*, 2012). CMIP5 includes a more comprehensive set of GCMs with more complexity run at higher spatial resolution with more complete representations of external forcings, scenario types, and diagnostic outputs in comparison to the CMIP3 models (Knutti and Sedláček, 2013) (Supporting Information Tables S1 and S2 for models used). The Expert Team on Climate Change Detection and Indices (ETCCDI) has defined a set of climate indices that focus on moderate extremes based on daily minimum temperatures, maximum temperatures, and precipitation. These CMIP5 extreme indices were downloaded from the ETCCDI archive (available at http://www.cccma.ec.gc.ca/data/climdex/), whereas the CMIP3 indices used in this study were computed by individual modelling centres based on the definitions of Frich *et al.* (2002) (available at http://www.pcmdi.llnl.gov). In this study, simulations and extreme indices of 23 models from CMIP5 archive and 9 medium and higher resolution models from CMIP3 archive are analysed for the 20th century historical experiment, and for multiple scenarios (B1, A1B, and A2 for CMIP3 and RCP 8.5 for CMIP5; Tables S1 and S2 for models used in this study). The respective greenhouse gas concentrations in 2100 are equivalent to 600, 850, 870 parts per millions carbon dioxide with emissions from human activities in B1, A1B, A2 scenarios and 1370 carbon dioxide equivalent in the RCP8.5 scenario (Moss *et al.*, 2010). Three indices that describe temperature-related extremes include the extreme temperature range, frost days, and warm nights. The remaining four indices describe precipitation extremes, which include consecutive dry days, 5-day precipitation, precipitation >95th percentile, and precipitation intensity (Table S3). Multi-model averages (MMA) and all other calculations were averaged for the bounding geographic coordinates defining the EH and WH regions.

2.2. Observed extreme indices from HadEX2 data set and ground stations

Observed extreme indices from the HadEX2 data set were used to provide density distributions for two periods (1960–1979 and 1980–2000), which also allowed evaluation of the modelled extreme indices. HadEX2 is a gridded land-based data set of indices of temperature and precipitation extremes based on global station data interpolated onto a $3.75° \times 2.5°$ longitude–latitude grid over the 1901–2010 period (Donat *et al.*, 2013). This data set is also calculated following the ETCCDI protocol and is available on the website http://www.climdex.org. Gridded temperature and precipitation data from the University of East Anglia Climate Research Unit (CRU-TS, v.3.0) were also used to compare simulated mean late 20th temperature and precipitation (Mitchell and Jones, 2005). Observed extreme indices for several stations across the HKH were also used to identify trends in all seven temperature- and precipitation-related indices. A total of five stations with long-term (1960–2000) precipitation and temperature indices were selected for the analysis of observational data (Figure 1). Four stations fall within the EH region: Pagri (27.73°N/89.08°E, 4300 m), Xigaze (29.25°N/88.88°E, 3837 m), Nedong (29.23°N/91.77°E, 3657 m), and Okhaldhunga (27.3°N/86.5°E, 1720 m). One station, Gilgit (35.92°N/74.33°E, 1459 m) lies in the WH region. Temperature and precipitation extreme indices were calculated only for Okhaldhunga to extend over the years 1960–2000, which were derived using a software package (RClimDex) written in R software (ETCCDI; http://cccma.seos.uvic.ca/ETCCDI/software.shtml). The trends in all observed climate indices were identified and tested for statistical significance at the 95% confidence level using the Mann–Kendall (MK) test for trend (Mann, 1945; Hipel and McLeod, 1994). Density plots of observed climate indices were also computed for the years 1960–1979 and 1980–2000 at all stations, for qualitative comparison with simulated indices and for analysing any shifts in distributions. Kolmogorov–Smirnov (KS) tests (Massey, 1951) were used to determine whether these distributions were significantly different from one another.

2.3. Density plots of extreme indices for CMIP3 and CMIP5

Density plots of MMAs of simulated annual extreme indices were computed for late 20th century (1970–1999) and 21st century (2020–2049 and 2070–2099) periods for both CMIP3 and CMIP5 datasets. For consistency, density plots for the 20th century use the same models as the 21st century density plots. Additionally, KS tests were used to determine whether the middle (2020–2049) and late (2070–2099) 21st century distributions of simulated extreme indices were significantly different from the late 20th century (1970–1999) distribution.

2.4. Time evolution of changes in CMIP3 indices

We carried out an extended set of analyses using the CMIP3 data set, which included time evolution of changes in simulated indices and percent changes by the 21st century in multi-model projected monthly mean temperature and precipitation. Multi-model ensemble time series of extreme indices for the 1901–2099 period, averaged over each region, were evaluated for CMIP3 models following the methodology by Tebaldi *et al.* (2006). A complete time series of each index and scenario was produced for the 1901–2099 period by combining the 20th and 21st century runs. The time series were standardized, and anomalies were computed with respect to the base period of 1961–1990. The base period was detrended by removing the least-squares linear trend, and the standard deviation was computed for this detrended base period. Anomalies for the entire period were standardized by the standard deviation of the detrended base period, and MMAs were computed for all indices across all scenarios. The multi-model ensemble average time series of the extreme indices (regionally averaged) were also smoothed with a 10-year running average, indicating the direction of change. The width of 1 standard deviation around the ensemble mean was used to represent inter-model variability.

2.5. Twenty-first century changes in temperature and precipitation

We additionally computed changes in the annual cycles of temperature and precipitation using the same set of model simulations used in the analysis of extreme indices. Simulations of monthly temperature and precipitation for the 20th and 21st centuries using the SRES B1, A1B, and A2 scenarios were utilized for this analysis. Precipitation differences were calculated for the middle (2020–2049 minus 1970–1999) and late (2070–2099 minus 1970–1999) 21st century and were standardized by the late 20th century standard deviation of each model. The multi-model mean monthly differences between the middle or late 21st century and the late 20th century period were tested for their statistical significance. These 20th and 21st century distribution differences were first assessed for normality (Shapiro–Wilk test). F-tests were then used to compare the variances between normally distributed 20th and 21st century samples. Two sample t-tests were determined appropriate for normally distributed samples. For non-normally distributed samples, differences in multi-model mean precipitation and temperature were tested for statistical significance using Wilcoxon tests. All significance tests were performed at the 95% confidence level.

3. Results

3.1. Mean climatology over EH and WH regions

The annual cycles of temperature and precipitation for both regions show similar patterns in both CMIP3 (Figure 2) and CMIP5 (Figure S1) groups of models. The annual cycle of temperature is well represented by both CMIP generation models in the EH region, with most of the models overestimating temperature by approximately 0.4 °C compared with CRU data in the EH region across all months (Figure 2(a)). On average, the EH temperatures range from −0.70 °C in winter to 13.6 °C in summer over the 1970–1999 period. There is a large cold bias by CMIP models in the WH region and temperatures are underestimated by as much as approximately 3.9 °C, particularly through winter months (Figure 2(b)). The WH region shows greater seasonal variability in temperature, with average winter temperatures approximately −9.6 °C and average summer temperatures approximately 11.9 °C. The MMA precipitation for the EH region follows CRU precipitation values closely but with greater inter-model variability during the monsoon period (May to October) (Figure 2(c)). There is a wet bias throughout the year in the WH region across CMIP3 models. The MMA precipitation overestimates CRU precipitation in the WH region by approximately 1.1 mm day^{-1} on average across all months (Figure 2(d)). The precipitation in the EH region shows a strong seasonal cycle with most precipitation falling in the monsoonal months (9.8 mm day^{-1} on average), while WH receives on average 1.3 mm day^{-1} with only a small seasonal variability.

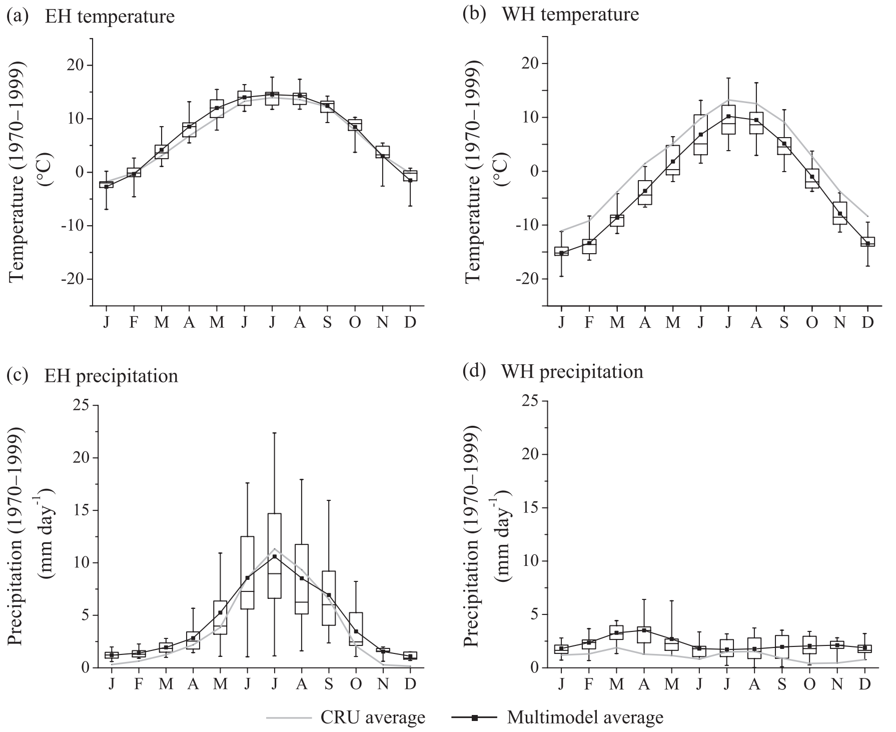

Figure 2. Multi-model average CMIP3 for late 20th century (1970–1999) for temperature (°C) and precipitation (mm day^{-1}) compared with CRU gridded observations for the EH and WH regions. The box represents the interquartile range where multi-model averages and median values are represented by black squares and horizontal lines, respectively. The whiskers represent the minimum and maximum model values.

Table 1. Trends in observed annual temperature and precipitation-related extreme indices at stations in the Hindu Kush-Himalaya region for 1960–2000, as shown by Kendall's τ statistic.

Station	Xtemp range	Frost days	Warm nights	Dry days	5 days precip	Precip > 95th	Precip. intensity
Gilgit	0.014	0.085	**−0.44**	−0.053	0.054	0.04	−0.019
Nedong	**−0.282**	**−0.494**	**0.424**	−0.063	−0.028	−0.083	−0.026
Pagri	−0.039	*−0.200*	**0.43**	**−0.257**	0.083	0.16	0.146
Xigaze	−0.065	**−0.218**	**0.57**	−0.094	0.002	−0.08	0.045
Okhaldhunga	0.153	–	**0.44**	−0.123	−0.032	−0.04	0.027

Significance at the 95 and 90% confidence levels based on the Mann–Kendall trend test is indicated in boldface and italics, respectively.

3.2. Observed extreme indices

We utilized MK tests to assess the presence of overall trends for the 1960–2000 period in the observed extreme indices at all five meteorological stations (Figure 1 and Table 1). MK statistics at a 95 and 90% confidence levels indicate the absence of significant trends in three out of the four precipitation-related indices (5-day precip, precip >95th, and precip intensity). MK tests indicate decreasing trends for dry days across all stations, although significant only at Pagri. The trends in precipitation-related indices also lack any consistent pattern across the five stations. In contrast, all temperature-related extreme indices exhibit significant trends across one or more stations (Table 1).

Three EH stations (all located at elevations above 3500 m) exhibit declining trends in the xtemp range (although significant only at Nedong; Table 1). In contrast, Gilgit (Figure 3(a)) in the WH region and Okhaldhunga at a lower elevation in the EH region (Figure 3(m)) exhibit positive shifts in xtemp range. Density plots of xtemp range show a negative shift from the 1960–1979 to the 1980–2000 period at Nedong, consistent with observed declining MK trend statistic over this time period (Figure 3(d)). Density plots of xtemp range at Gilgit suggest higher variability for the 1980–2000 distribution, while the remaining stations show no clear, observable shifts in distributions (Figure 3(a), (g), and (j)).

The MK tests for trend reveal significant negative trends for the number of annual frost days at Nedong, Xigaze (significant at 90% confidence level), and Pagri (Table 1), with the exception of Okhaldhunga (where frost days were not calculable by definition since temperature does not fall below 0 °C) and Gilgit (which exhibits a positive trend in the WH region; Figure 3(b)). On average, stations at higher elevations exhibit greater total numbers of frost days relative to stations at lower elevations, with Pagri (4300 m) experiencing on average approximately 240 frost days per year over the 1960–2000 period and Gilgit (1459 m) experiencing on average only approximately 70 frost days per year over the same period (Figure 3(b) and (h)). Stations lying in the mid-elevational range

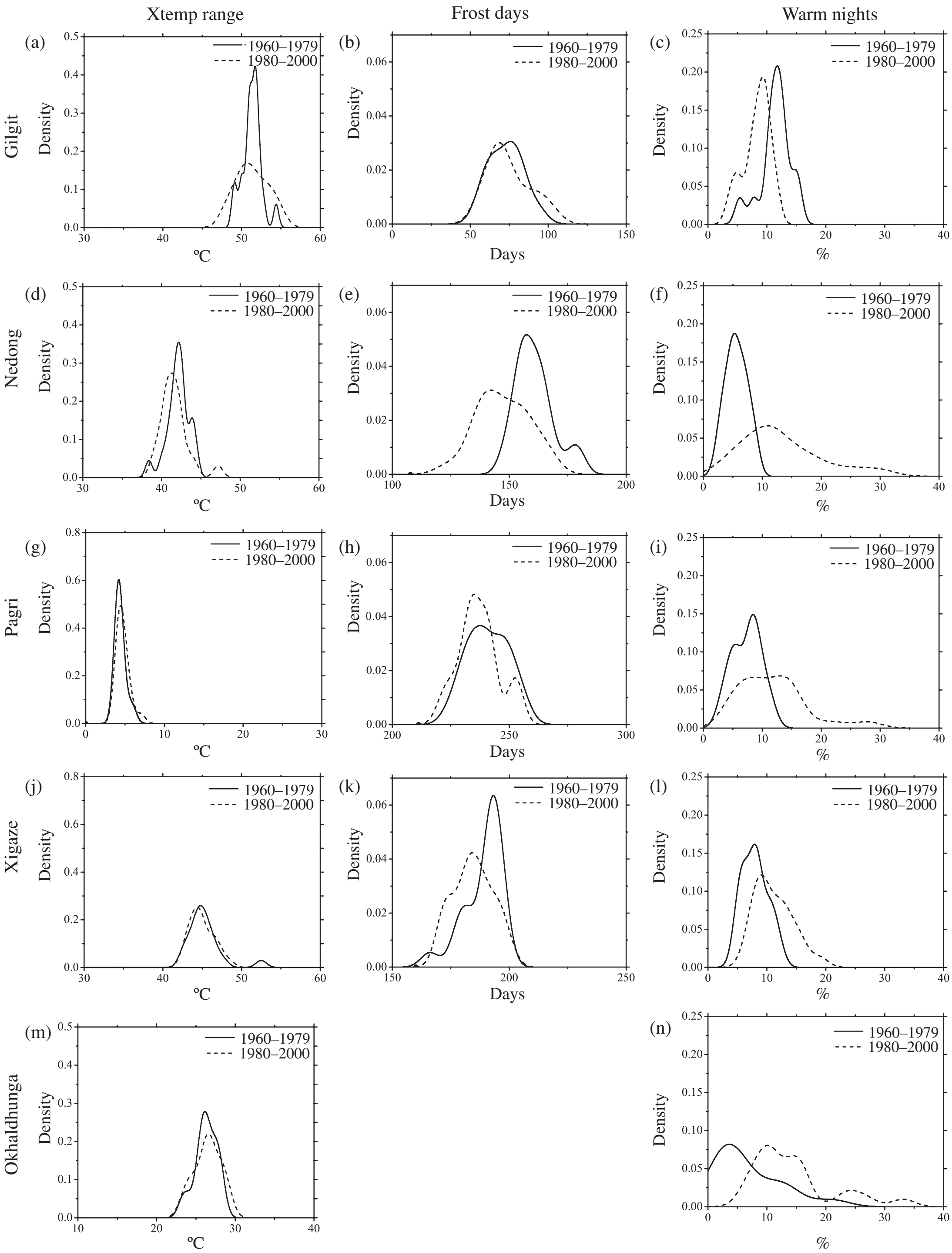

Figure 3. Probability density functions of xtemp range (a, d, g, j, and m), frost days (b, e, h, and k), and warm nights (c, f, i, l, and n) for Gilgit (a–c), Nedong (d–f), Pagri (g–i), Xigaze (j–l), and Okhaldhunga (m and n) meteorological stations (see Figure 1 for locations). The 1960–1979 (solid line) and 1980–2000 (dashed line) periods are shown for the 20th century.

(3600–3800 m) exhibit the largest decrease in the occurrence of frost days, with Nedong showing a decrease of approximately 20 annual frost days from the 1960–1979 to 1980–2000 period (Figure 3(e)). KS tests reveal significantly different distributions of frost days when comparing the two 1960–1980 and 1980–2000 periods for Nedong only, which is consistent with the stronger MK trend statistic at this station.

Warm nights across all stations in the EH region exhibit significant positive shifts (Figure 3(f), (i), (l), and (n)), while Gilgit in the WH region exhibits a significant negative shift (Figure 3(c)). This is consistent with the significant positive trends observed over the 1960–2000 period across the EH stations (Table 1). The KS tests did not show any other statistically significant differences in the distribution of temperature and precipitation-related indices between the two late 20th century periods. The 1980–2000 distributions of precipitation intensity do not exhibit any significant shifts across the stations, while the distributions for precip >95th percentile indicate a slight negative shift at Nedong, Xigaze, and Okhaldhunga as well as a positive shift at Pagri for this period (not shown in Figure 3). Density plots of dry days (not shown in Figure 3) suggest negative shifts over the 1980–2000 period for Okhaldhunga, Pagri, and Xigaze; however, these distributions are not significantly different from the 1960–1979 samples according to KS tests.

Observed changes in HadEX2 extreme indices for both temperature and precipitation based indices are also shown by density plots for the EH and WH regions (Figure 4). Most indices show shifts from the 1960–1979 period to the 1980–2000 period. Particularly, xtemp range shows negative shifts and warm nights show positive shifts for both regions consistent with the analysis of observed stations indices. Density plots of precipitation indices from HadEX2 are less coherent than temperature-based indices as also shown in the previous analyses of extreme indices based on station observations. KS tests showed significant shifts at the 95% confidence level for dry days, xtemp range, frost days, and warm nights for the EH region. For the WH region, only xtemp range and warm nights showed significant shifts at the 95% confidence level between the two periods.

3.3. Simulated temperature-related extreme indices

Both the CMIP5 and CMIP3 data sets are cold biased relative to HadEX2 as they show larger numbers of frost days (cold extremes) particularly in the WH region (Figures 4–7 and S2(a)). Since the 20th century simulated frost days are greater than those observed from HadEX2, the future reduction in frost days might also be overestimated by model projections. The models also disagree with HadEX2 for xtemp range with both the CMIP5 and CMIP3 distributions showing much larger values than the observations. The CMIP models compare well with HadEX2 in the late 20th century distribution of warm nights for both EH and WH regions. Poor observational network coverage particularly in the higher elevations is used to produce the HadEX2 data set, and the inability of the models to resolve processes in high altitude terrain leads to biases in comparison of models to observations particularly in high elevation regions such as the Himalaya and Tibetan Plateau (Donat *et al.*, 2013).

Projected shifts in CMIP5 MMA indices for the 21st century (2020–2049 and 2070–2099) indicate significant shifts outside the current ranges in all temperature-related indices, particularly in frost days (Figure 5(b) and (h)) and warm nights (Figure 5(c) and (i)) for both regions. Density plots of CMIP3 MMA temperature-related indices for the EH (Figure 6(a)–(i)) and WH (Figure 7(a)–(i)) regions also indicate similar shifts to those of CMIP5 by mid and late 21st century. KS tests revealed that the distributions of frost days and warm nights for the middle and late 21st century are significantly different from late 20th century distributions in all scenarios for both the EH and WH regions. MK tests for trend exhibit significant ($p < 0.05$) positive trends for simulated warm nights, while xtemp range and frost days indicate significant negative trends ($p < 0.05$) (Figures 8 and 9). These simulated trends in extreme climate indices are consistent with the projected changes of approximately 2–4 °C in temperatures for the two regions by late 21st century (Figures 10 and 11).

The distributions of mid and late 21st century xtemp range are significantly different from late 20th century distributions in all scenarios in the EH region ($p < 0.05$), while they are significantly different by the late 21st century in all scenarios in the WH region. Density plots of MMA xtemp range exhibit more pronounced negative shifts by the middle and late 21st century in the EH region (Figures 5(a) and (g) and 6(a)–(c)) as compared with the WH region (Figures 6(a) and (g) and 7(a)–(c)). Time evolution of area-averaged CMIP3 indices indicate a decrease in the xtemp range by the end of the 21st century in both regions (Figures 8(a) and 9(a)). This is consistent with the declining trends already apparent in the significant negative trend in the xtemp range in the EH region from station observations and HadEX2 indices (see Section 3.2). The largest decrease in xtemp range (as indicated by a 10-year running average) is approximately 1.3 standard deviations (SD) in the A2 scenario for the EH region (Figure 8(a)), which is greater than the largest decrease in the A2 scenario for the WH region (which by comparison is only approximately 0.8 SD; Figure 9(a)).

Both regions also exhibit a decrease in annual frost days by the 21st century in RCP 8.5 (CMIP5) (Figure 5(b) and (h)) and three SRES scenarios (CMIP3) (Figures 6(d)–(f) and 7(d)–(f)). However, models may be underestimating frost days in the WH, which is inconsistent with the positive shifts in frost days from the middle to late 20th century observed at Gilgit. Simulated frost days indicate that on average, the EH region has fewer number of frost days (approximately 150 for the 20th century) compared with the WH region (approximately 280 for the 20th century). The distributions of frost days in the late 21st century for both regions exhibit no overlap with 20th century distributions, suggesting that the highest number of annual frost days in the late 21st century will be less than the lowest number of annual frost days in the 20th century.

Simulations for the 21st century indicate dramatic increases in warm nights in both CMIP3 and CMIP5 datasets across all scenarios (Figures 5(c) and (i), 6(g) and (i), and 7(g) and (i)). The 21st century simulations indicate a shift to more warm nights in all scenarios and by the late 21st century, the distributions of warm nights for both regions do not display any overlapping values with the 20th century distributions. On average, the EH region exhibits a shift towards more warm nights in the 21st century when compared with the WH region for all scenarios.

3.4. Simulated precipitation-related extreme indices

Both CMIP model generations agree well with the HadEX2 data for 5-day precipitation and precip >95th

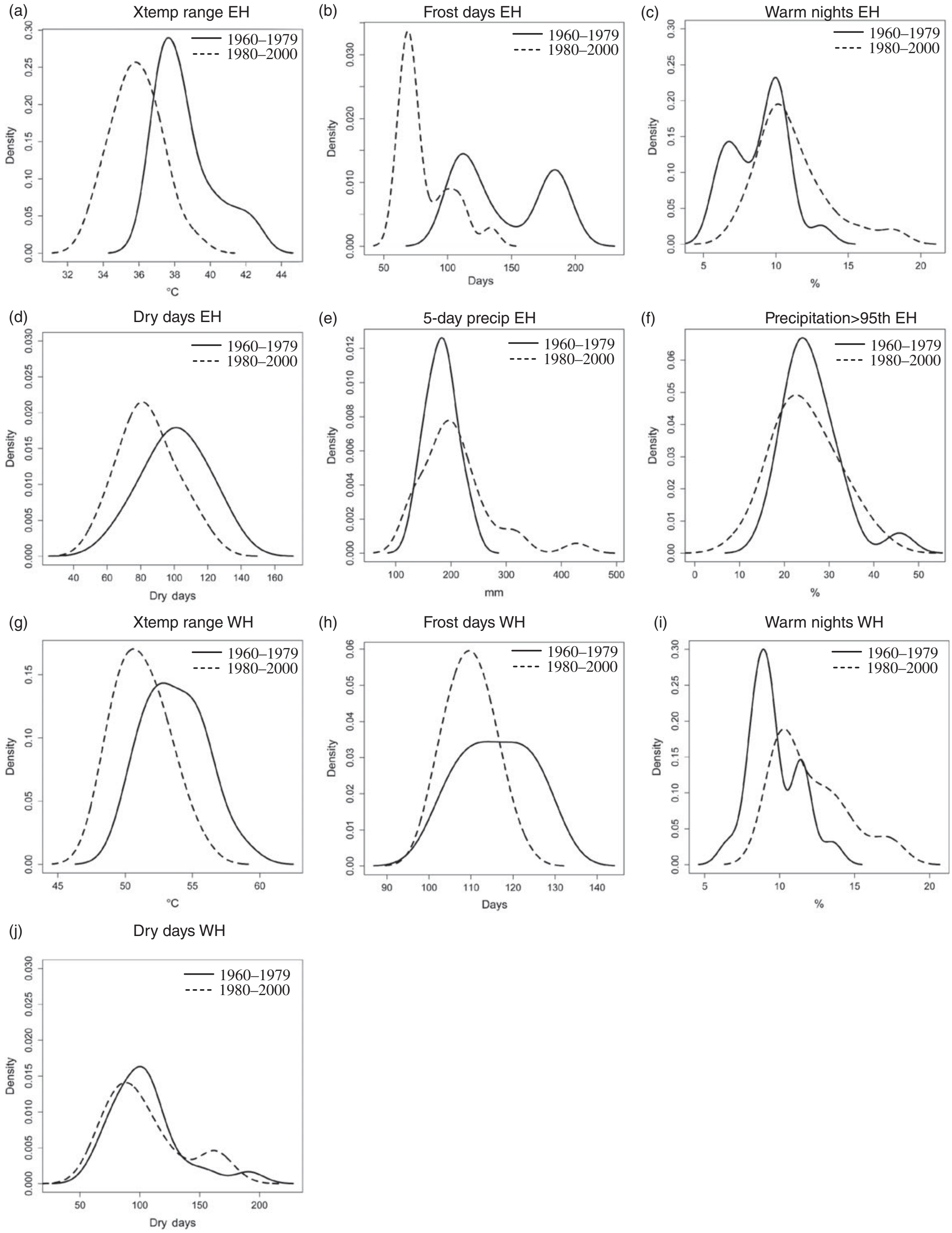

Figure 4. Change in distributions for HadEX2 indices for EH (a–f) and WH (g–j) regions. We show distribution of indices for two periods [1960–1979 (black) and 1980–2000 (dashed)] for xtemp range, frost days, and warm nights; 5-day precip and precip >95th percentile indices are not available for the WH region.

percentile (Figures 4–7). This is consistent with the findings of Sillmann *et al.* (2013b) at the global and regional scales. Both CMIP3 and CMIP5 models disagree with the HadEX2 data set for consecutive dry days with the models showing almost twice as few dry days in both regions. The underestimation of dry days by CMIP5 models when compared with HadEX2 has also been observed in several regions (Figures 5(d) and (j), 6(j)–(l), 7(j)–(l), and S2(b)) (Sillmann *et al.*, 2013b). Shifts in precipitation indices in CMIP3 and CMIP5 data sets indicate wetter conditions with more frequent precipitation extremes particularly for the EH region. For both regions, all modelled precipitation-related extreme indices exhibit significant increasing trends confirmed by the MK tests for trend. The results indicate that the increase in precipitation for

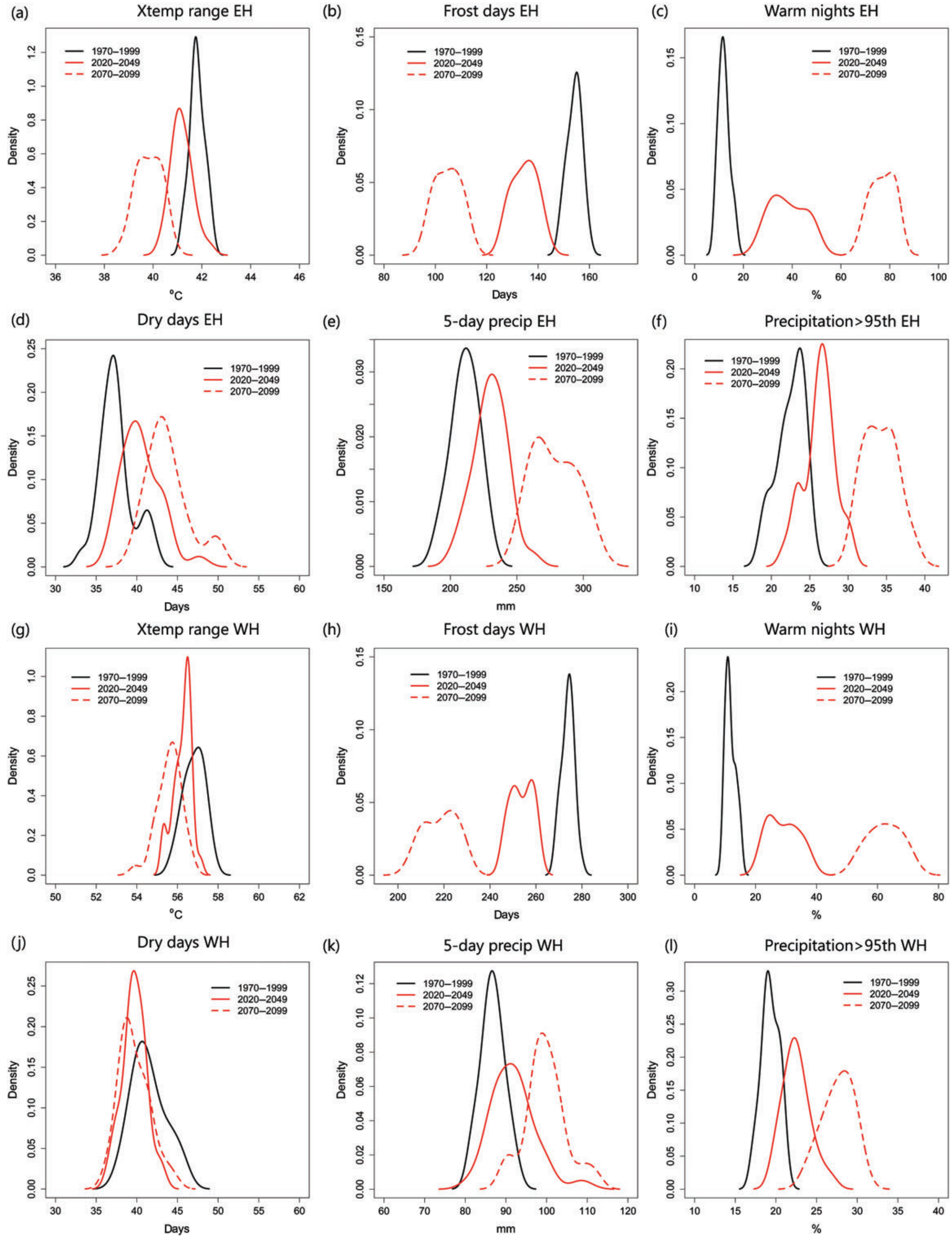

Figure 5. Change in distributions for CMIP5 multi-model average historical (1970–1999) and RCP 8.5 projected scenarios (2020–2049 and 2070–2099) for simulated xtemp range, frost days, warm nights, dry days, 5-day precip, and precip >95th for the EH (a–f) and WH (g–l) regions.

these regions is due to increased frequency of extreme precipitation events.

CMIP5 MMA density plots indicate a significant positive shift in dry days in RCP 8.5 scenario for the EH region (Figure 5(d) and (j)). CMIP5 MMA distributions show a negative shift in dry days for the WH region contradicting CMIP3 MMA distributions (Figure 7(j)–(l)). CMIP3 density plots indicate that dry days show little change for the WH region during the 20th century (Figure 7(j)–(l)). However, the distribution in dry days shows a positive shift in the A1B (Figures 6(k) and 7(k)) and A2 (Figures 6(l) and 7(l)) scenarios for both regions by the end of the 21st century. On average, simulated time series of dry days index shows much higher temporal variability compared with other indices. By the updated ETCCDI definition, the length of the multiyear dry spells is assigned to the year

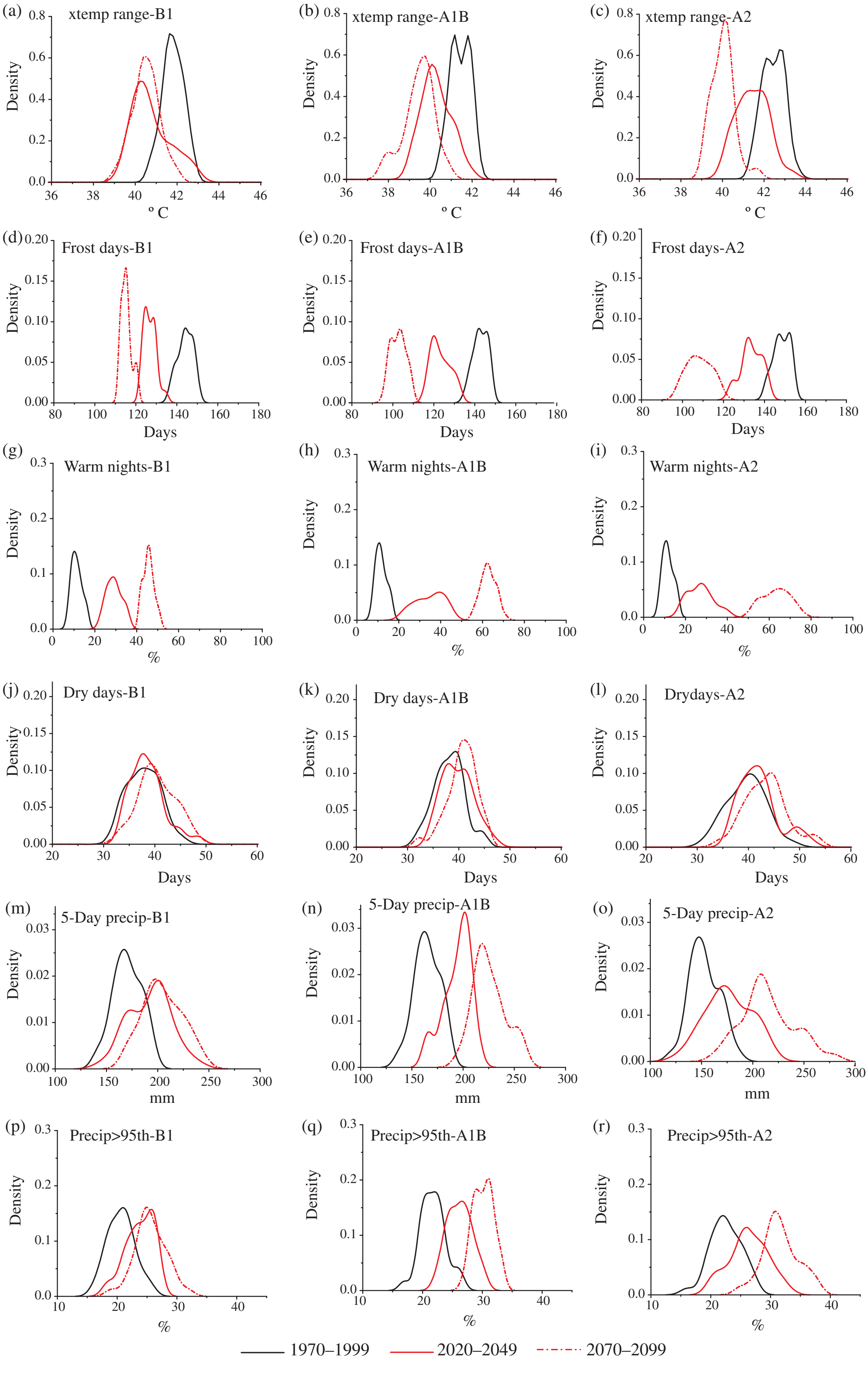

Figure 6. Density plots of CMIP3 multi-model averages showing changes in the distribution of temperature- and precipitation-related extreme indices for the EH region. Late 20th century period (1970–1999) is compared with projections for the middle and late 21st century for each scenario [SRES B1 (a, d, g, j, m, and p), SRES A1B (b, e, h, k, n, and q), and SRES A2 (c, f, i, l, o, and r)].

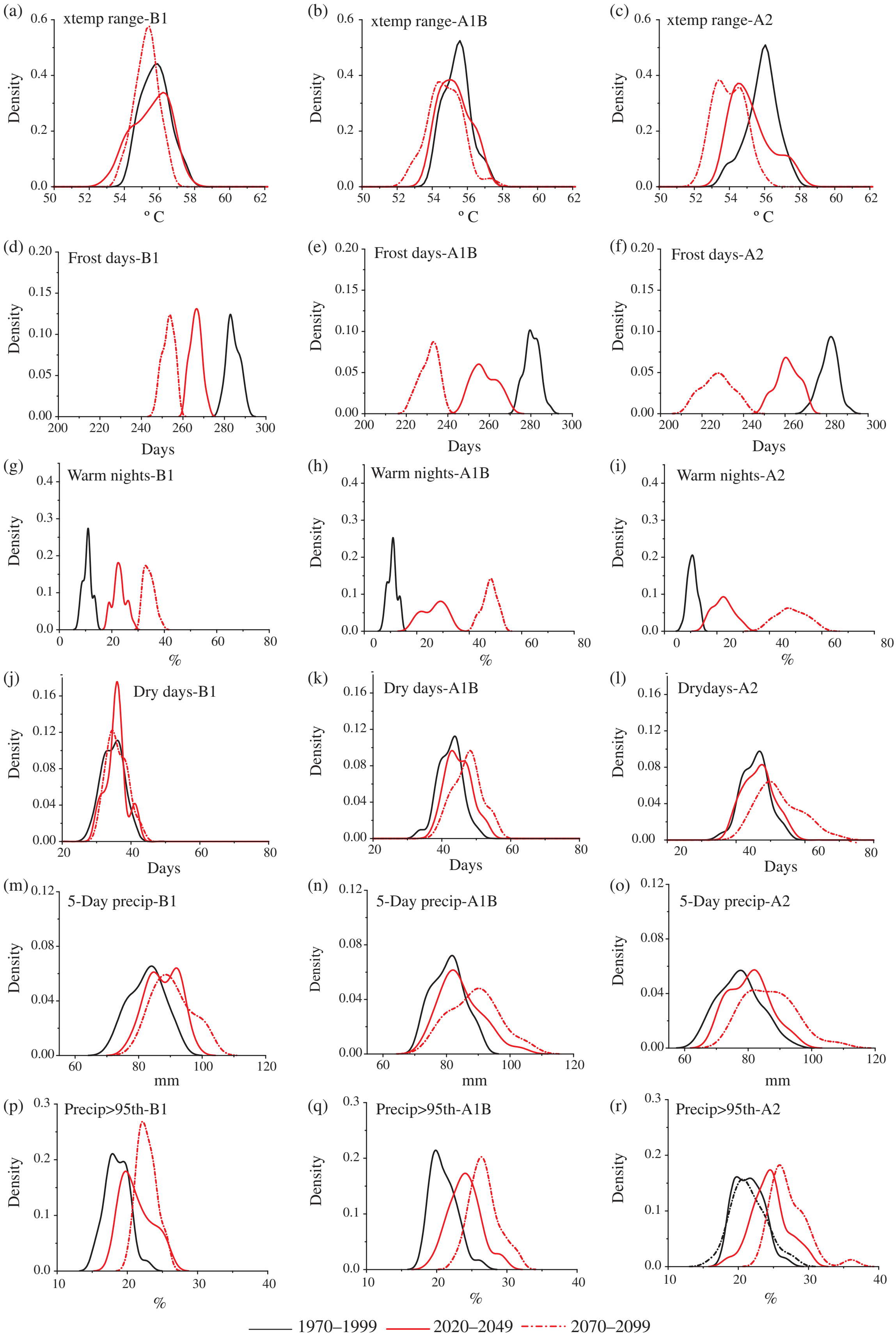

Figure 7. Density plots of CMIP3 multi-model averages showing changes in the distribution of temperature- and precipitation-related extreme indices for the WH region. Late 20th century period (1970–1999) is compared with projections for the middle and late 21st century for each scenario [SRES B1 (a, d, g, j, m, and p), SRES A1B (b, e, h, k, n, and q), and SRES A2 (c, f, i, l, o, and r)].

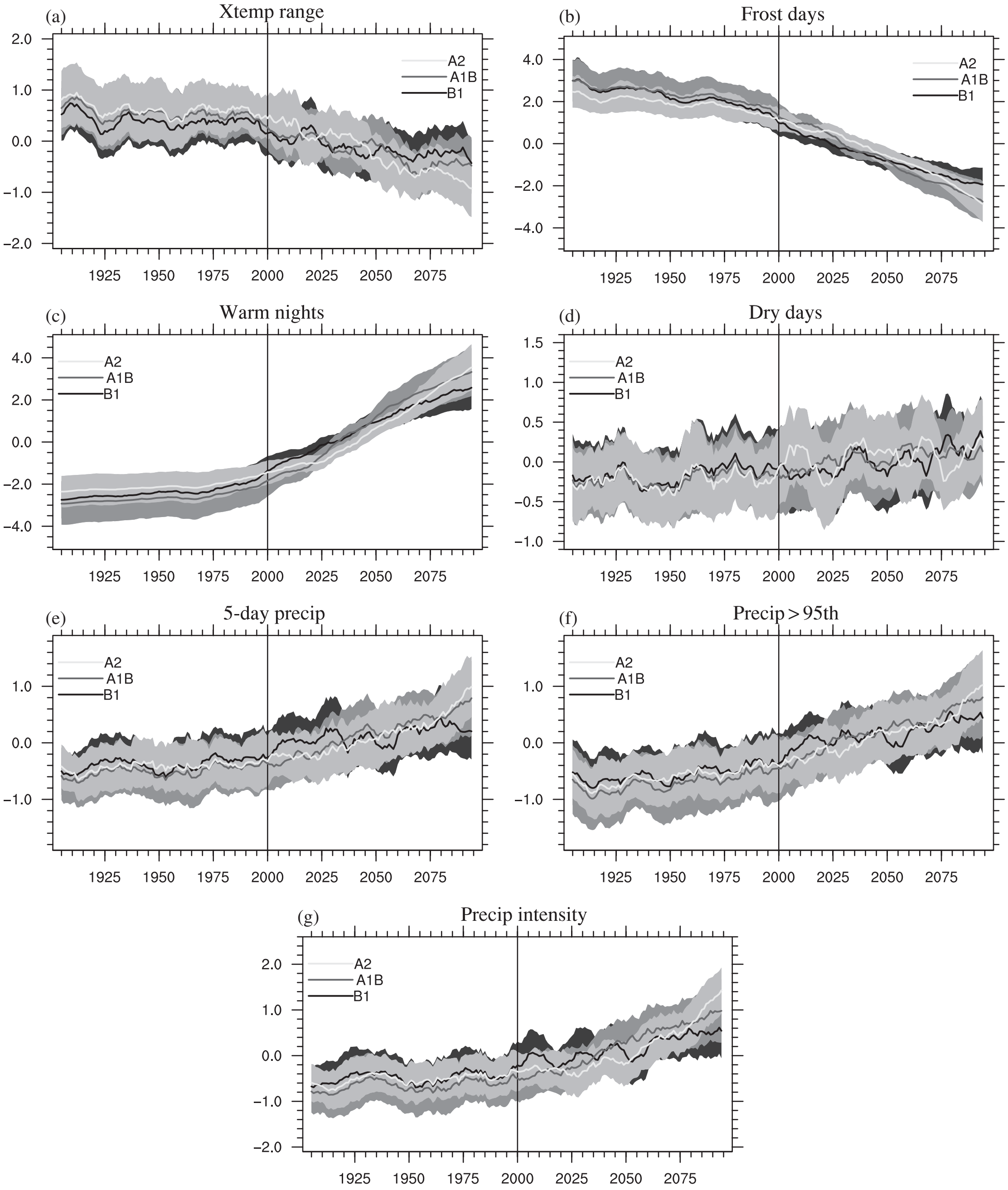

Figure 8. Simulated time series of standardized temperature and precipitation-related CMIP3 extreme indices anomalies over 1901–2099 for the EH region. The thick lines indicate the 10-year running average. Shading represents the width of 1 standard deviation of the ensemble mean. The 21st century scenarios are shown for the B1 (dark gray), A1B (medium gray), and A2 (light gray) scenarios.

when the spell ends such that very large dry spells affect the spatial averages leading to large interannual variability (Sillmann *et al.*, 2013b). CMIP3 dry days indices used in this study are always terminated at the year's end, in contrast to the CMIP5 dry spells where accumulated dry days are carried across the calendar year when the spell ends (Sillmann *et al.*, 2013b). Dry days index describes the lower tail of the precipitation distribution and change and trends of changes in dry days are smaller compared with the shifts in other climate indices. The 21st century density distributions overlap with the 20th century distributions for dry days, and the changes are difficult to interpret as the interannual variability together with inter-model variability confounds the actual changes.

Both CMIP3 and CMIP5 distributions of 5-day precip indicate projected increases across all scenarios by the 21st century (Figures 5(e) and (k), 6(m)–(o), and 7(m)–(o)). CMIP5 scenario projects a greater shift in 5-day precip distributions by 21st century for both regions relative to the CMIP3 distributions. Overlapping distributions of 5-day precip for the WH region in CMIP3 scenarios between the 20th and 21st century suggest smaller changes as projected by this multi-model data set. Both CMIP3 and CMIP5 density plots of 5-day precip indicate positive

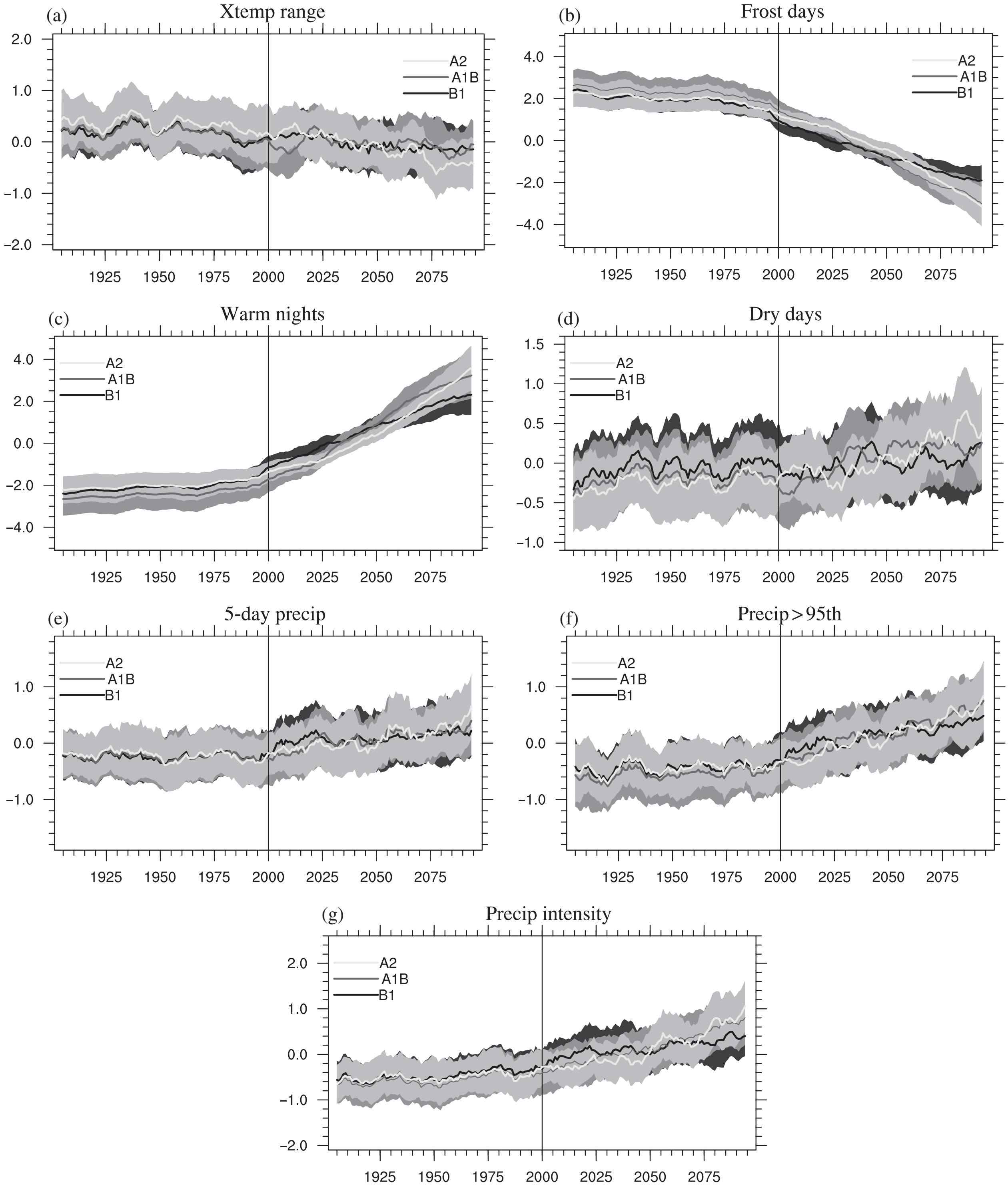

Figure 9. Simulated time series of standardized temperature and precipitation-related CMIP3 extreme indices anomalies over 1901–2099 for the WH region. The thick lines indicate the 10-year running average. Shading represents the width of 1 standard deviation of the ensemble mean. The 21st century scenarios are shown for the B1 (dark gray), A1B (medium gray), and A2 (light gray) scenarios.

shifts to higher precipitation and greater variability in the EH region compared with the WH region in all middle and late 21st century scenarios (Figures 8(e) and 9(e)).

Long-term simulations by CMIP3 and CMIP5 models indicate positive shifts in precip >95th percentile by the end of the 21st century in both regions (Figures 6(p)–(r) and 7(p)–(r)). Precip intensity shows an increasing trend by the late 21st century across all scenarios in both regions (Figures 8(g) and 9(g)). However, MMA density plots indicate overlap in a majority of 20th and 21st century distributions for both regions, suggesting increases in precipitation intensity are relatively small (not shown). CMIP3 models indicate that the distributions of precipitation intensity

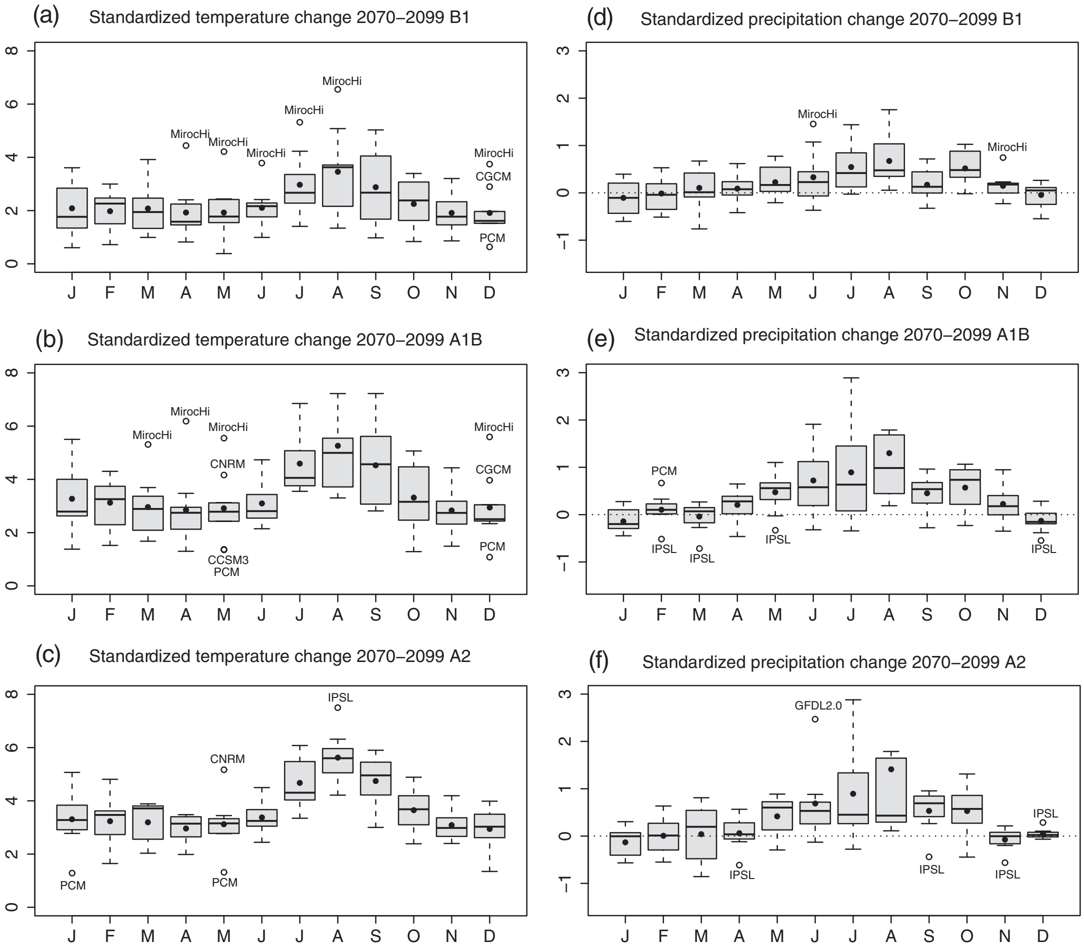

Figure 10. Box plots show CMIP3 multi-model statistics for standardized monthly temperature (a–c) and precipitation (d–f) differences for the EH region (late 21st century minus 1970–1999) for SRES B1, A1B, and A2. The interquartile range (IQR) is shaded and horizontal black lines represent multi-model median values. Multi-model averages are represented by black circles. The whiskers represent the furthest model value within 1.5 times the IQR. Open circles represent outliers.

for the 21st century are not significantly different for both regions except in the A2 scenario.

3.5. Changes in annual cycles of temperature and precipitation

The 21st century CMIP3 and CMIP5 projections of xtemp range, frost days, and warm nights are consistent with the projected changes in annual cycles of temperature. Temperature differences from the late 20th century to the middle and late 21st century are significant across all scenarios in both regions (Figures 10–12 and S3–S5). The projected annual average temperature increases by the end of the 21st century range from 2.5 to 4.0 °C for the EH region, and from 2.8 to 4.5 °C for the WH region. Both the CMIP3 and CMIP5 model generations project temperature increases of similar magnitude for the late 21st century. The late 21st century standardized temperature changes indicate greater inter-model variability in the magnitude of the temperature increase, particularly during the summer months (July to September) for the EH region in both CMIP3 and CMIP5 model projections.

MMAs suggest a statistically significant tendency towards increased precipitation during the monsoon season (April to October) in both the middle and late 21st century in the EH region, also consistent with the increases in precipitation-related extremes (Figure 10). By the late 21st century, monsoonal precipitation changes are larger during April to August in the EH region but with increased inter-model variability across all scenarios. Changes in the late 21st century precipitation using CMIP5 models indicate increases starting in April, suggesting an earlier onset and longer monsoon season for the EH region when compared with CMIP3 model projections (Figure 12). Precipitation is expected to increase significantly during the monsoon season within the EH region, with an annual average increase of approximately 15–27% by the late 21st century. Multi-model projected precipitation changes indicate significant precipitation declines during January for the EH region. In contrast, the WH region only experiences on average a approximately 1–5% increase (statistically significant across all scenarios) in annual precipitation by the late 21st century, primarily owing to the combination of suppressed summer precipitation and increased winter precipitation (which is statistically significant during the months of December and January). It is likely that less frequent but heavier rainfall events do not

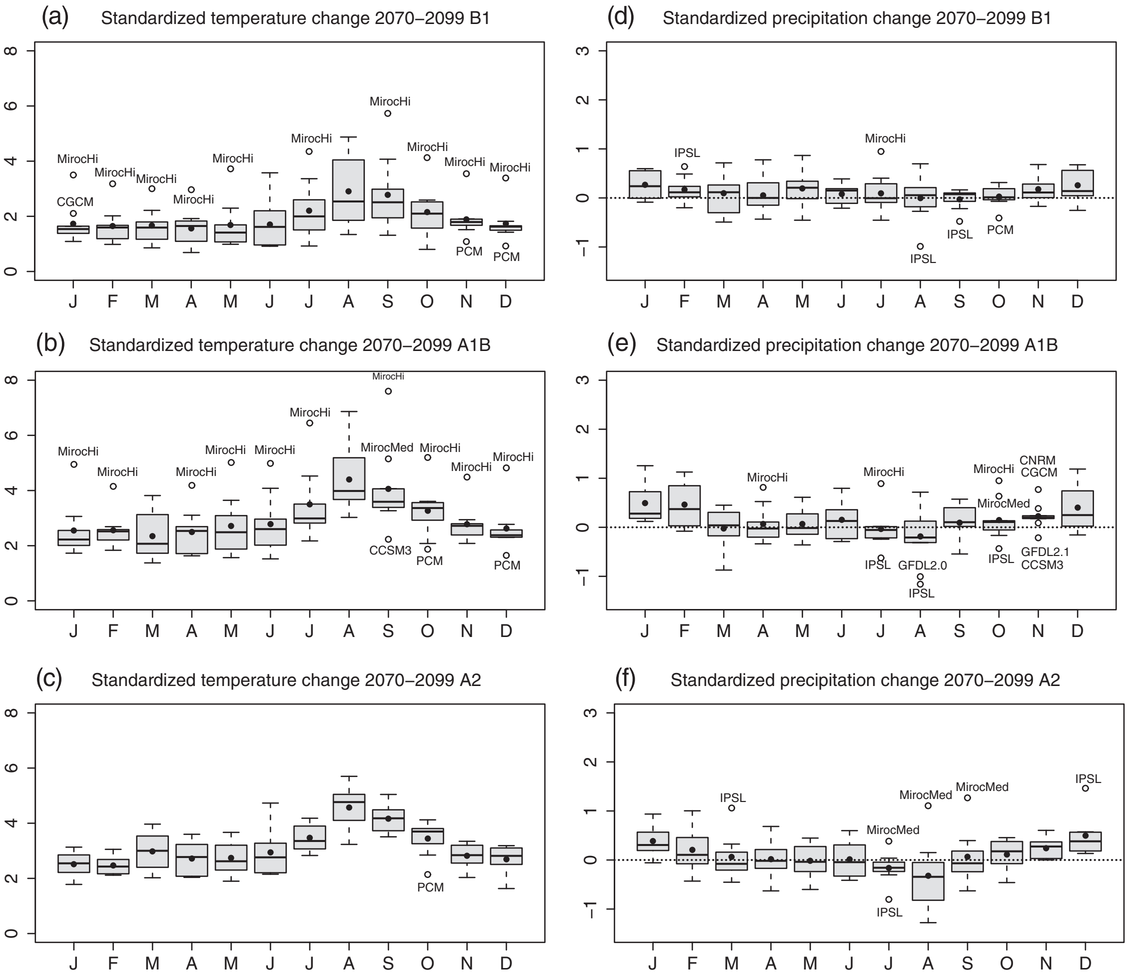

Figure 11. Box plots show CMIP3 multi-model statistics for standardized temperature (a–c) and precipitation (d–f) differences for the WH region (late 21st century minus 1970–1999) for SRES B1, A1B, and A2. The interquartile range (IQR) is shaded and horizontal black lines represent multi-model median values. Multi-model averages are represented by black circles. The whiskers represent the furthest model value within 1.5 times the IQR. Open circles represent outliers.

affect the total precipitation amounts in the WH region. Previous studies have shown precipitation intensity and heavy precipitation events to increase more than mean precipitation under a warming climate due to increases in atmospheric water vapour content (Tebaldi *et al.*, 2006; Scoccimarro *et al.*, 2013). In contrast, the significantly larger changes in the monsoon-season precipitation in EH region leads to significant changes in the total annual precipitation for that region. The CMIP5 models project consistent increases in precipitation across all months in RCP 8.5 when compared with the SRES A2 projections from CMIP3 models (Figures 11 and 12). Standardized precipitation changes for late 21st century for the WH region indicate less model variability relative to the late 21st precipitation changes in the EH region (Figure 11).

4. Discussion

Multi-model analyses indicate a continued trend for more extremes consistent with a warming climate particularly for temperature-related extreme indices. Temperature shifts by the middle to late 21st century are statistically significant across all scenarios and RCP 8.5 for both the EH and WH regions. A thorough comparison on SRES scenarios and RCPs is challenging and possible only if results are computed by the exact same set of models. Rogelj *et al.* (2012) indicate that the radiative forcings prescribed in CMIP3 and CMIP5 scenarios can lead to different temperature responses that also manifest as differences in temperature and precipitation extremes. This study shows that for the EH and WH regions, both the CMIP3 and CMIP5 models show good agreement with HadEX2 observations for warm nights, 5-day precip and precip >95th percentile. Both model generations are cold biased relative to observations showing a larger number of frost days, while they show almost twice as less dry days in both regions relative to HadEX2 observations. Sillmann *et al.* (2013b) have shown that for temperature indices the performance of CMIP3 and CMIP5 multi-model ensembles is comparable with respect to their ensemble mean. This study indicates that the spread amongst CMIP5 models for temperature-related indices is reduced compared with those by CMIP3 models, which was also observed by Sillmann *et al.* (2013a). However, CMIP5 models

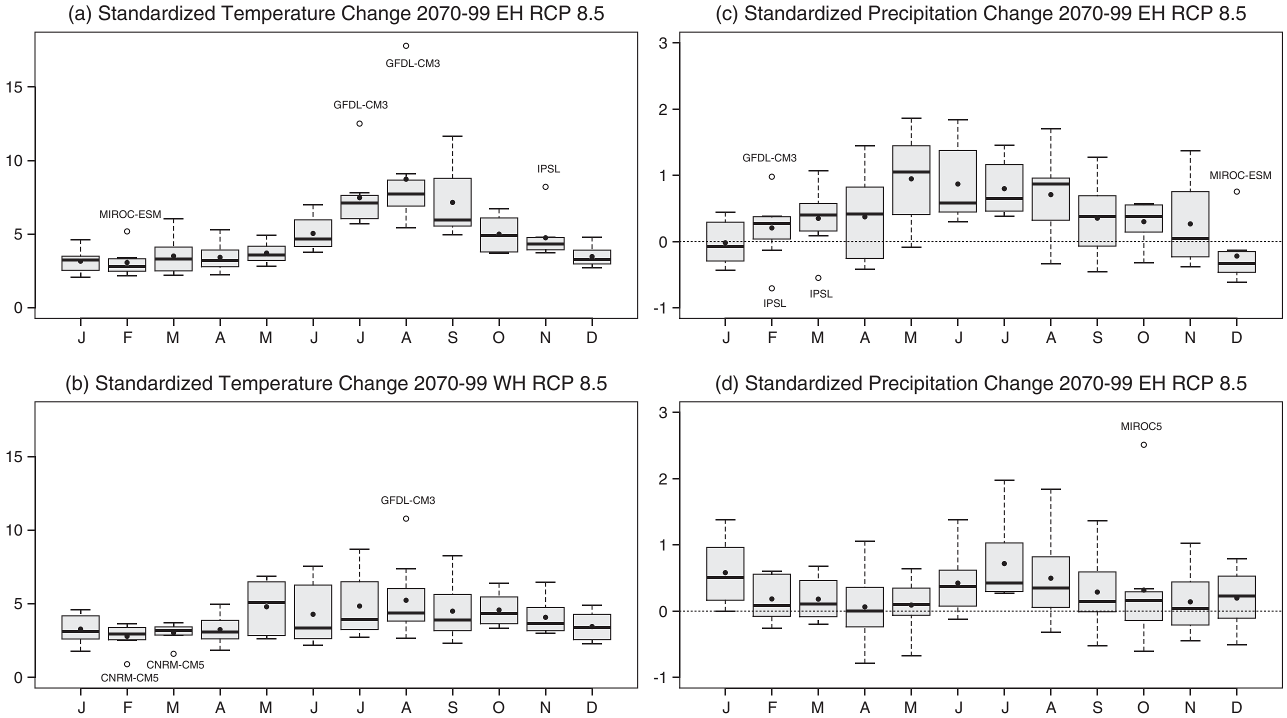

Figure 12. Box plots show CMIP5 multi-model statistics for late 21st century standardized monthly temperature and precipitation differences (late 21st century minus 1970–1999) for the EH region (a and c) and WH region (b and d) for RCP 8.5. The interquartile range (IQR) is shaded and horizontal black lines represent multi-model median values. Multi-model averages are represented by black circles. The whiskers represent the furthest model value within 1.5 times the IQR. Open circles represent outliers. Modern counterparts to the CMIP3 models used in this study, i.e. CCSM4, CNRM-CM5, GFDL-CM3, GFDL-ESM2G, IPSL-CM5A-LR, MIROC-ESM, MIROC5, and MRI-CGCM3.

tend to simulate more intense precipitation and fewer consecutive wet days than CMIP3 models and closer to the observations as represented by the HadEX2 indices, also shown by Sillmann *et al.* (2013b). This is indicative of an improvement in the CMIP5 model generation due to the higher spatial resolution. Model improvements in the parameterization of unresolved physical processes such as convective precipitation and improvements with respect to reproducing observed precipitation characteristics may play a role in precipitation simulations by CMIP5 being closer to observations as represented by the HadEX2 indices (Sillmann *et al.*, 2013b).

Changing climate extremes in these regions such as fewer frost days and more warm nights may negatively affect accumulation and increase the ablation of glaciers. Projections of glacier melt rates for the 2001–2030 period using CMIP3 climate models have indicated accelerated melting rates for the central Asian region (Ren *et al.*, 2007). Glacier mass balance projections for the Himalayan and Karakoram regions using CMIP5 models indicate a sixfold decrease from present by the 2080s under the high emission scenario of RCP8.5 (Chaturvedi *et al.*, 2014). Decreases of frost days are expected to be greater near the climatological mean position of the 0 °C isotherm (Meehl *et al.*, 2004) and, therefore, regions near this boundary should experience greater decreases in frost days.

With respect to precipitation-related indices, statistical tests indicate changes consistent with a wetter climate. Projected increases in 5-day precip, precip >95th percentile, and precip intensity, along with the precipitation projections for the annual cycle for the EH region, are indicative of an increased mean precipitation with more frequent extreme rainfall during the monsoon season. In the WH region, precipitation projections indicate small increases from October to February, indicative of a wetter cold season. Projected changes in annual cycles of temperature and precipitation also scale with emissions scenarios, with the higher emissions scenarios A1B and A2 tracking each other for most of the 21st century.

With regard to trends of climate extremes, our findings are similar to what has been observed globally indicative of intensification in temperature- and precipitation-based indices (Frich *et al.*, 2002; Alexander *et al.*, 2006; Sillmann *et al.*, 2013b). The significant increase in the annual occurrence of warm nights (as observed through instrumental records over this period) is consistent with the simulated CMIP3 and CMIP5 MMAs for both the EH and WH regions for the late 20th century in this study. Furthermore, observed significant declines in the annual number of frost days globally (Frich *et al.*, 2002; Alexander *et al.*, 2006) are consistent with the significant decreases in the observed and simulated MMA frost days for the EH and WH regions. Analyses of multi-model ensemble projections of extreme indices in the Tibetan Plateau, north of the Himalayan region, also indicate decreasing frost days and more frequent warm nights

(Yang *et al.*, 2012). Significant decreases in xtemp range are also reported in the analyses of extreme indices from improved global coverage (Alexander *et al.*, 2006). This declining trend in xtemp range is particularly notable in the EH region, largely owing to higher increases in minimum temperatures relative to increases in maximum temperatures (Frich *et al.*, 2002).

From a more regional perspective, regional-scale analyses of observed climate extreme indices for central and south Asia are presented by Klein Tank *et al.* (2006). In general, 70% of the meteorological stations in that region showed statistically significant increases in the percentage of warm nights observed for the 1961–1990 period, which may be part of a long-term trend persistent throughout the 20th century. Multi-model analyses from our study also simulate these increases in warm nights in both EH and WH regions and indicate further significant increases in the 21st century. The WH region exhibits increasing trends for warm nights in the late 20th century; however, the observed trend for warm nights at Gilgit shows a significant decreasing trend. At this station, the density plots exhibit more variability in xtemp range and higher probability of large numbers of frost days during the late 20th century. Statistically significant reductions in mean annual temperature since the 1960s (owing to summer cooling) have been reported in the Upper Indus Basin, whereas winter mean and maximum temperatures show statistically significant increases (Fowler and Archer, 2006). These contrasting signals of both warming and cooling in this basin have been thought to result from changes in large-scale circulation and feedback processes such as aerosol cooling (Yadav *et al.*, 2004; Fowler and Archer, 2006). In contrast to temperature-related extreme indices for the late 20th century, most regional indices of precipitation-related wet extremes showed no statistically significant trends regionally (Klein Tank *et al.*, 2006), which is also observed in the subset of EH and WH stations analysed in this study.

With regard to precipitation, our multi-model analyses indicate evidence for increases in monsoonal precipitation, as has also been demonstrated by other studies (Douville *et al.*, 2000; Seth *et al.*, 2011). Sen (2009) analysed extreme hourly precipitation patterns in India from 1980 to 2002 and found rising trends in extreme heavy precipitation events, particularly in the high-elevation regions of the northwestern Himalaya as well as along the foothills of the Himalaya. Projected changes in precipitation indices and annual cycles of precipitation indicate intensification of the monsoon, particularly in the EH region. In the WH region, projections of precipitation indices and annual cycle changes in precipitation indicate a wetter cold season. The largest increases in temperature for both regions (according to the A2 scenario) coincide with heavier precipitation projections in EH, but little change or small decreases in precipitation in the WH region. The prediction uncertainty from model uncertainty and scenario uncertainty is greater towards the end of the 21st century (Hawkins and Sutton, 2009) as shown by divergence among models particularly during the monsoon-season precipitation changes particularly in the EH region .The dominant contributions to prediction uncertainty in multi-decadal time scales are model and scenario uncertainty relative to uncertainty from internal variability of the climate system (Hawkins and Sutton, 2009). Although CMIP5 models exhibit improved inter-model agreement in their projections indicating increases in global monsoon area, precipitation, and intensity, models continue to exhibit substantial biases in the annual cycle of rainfall in monsoon regions (Seth *et al.*, 2013).

However, the South Asian summer monsoon remains a complex phenomenon influenced by several factors such as aerosols and black carbon (Lau *et al.*, 2006; Meehl *et al.*, 2008) and Eurasian snow–monsoon interactions (Peings and Douville, 2010); therefore, projected changes need to be taken with caution and demands detailed understanding of such processes and feedbacks.

The differences between the EH and WH regions in the behaviour of observed and modelled climate include a large cold bias for temperature in the WH region for the late 20th century. Multi-model ensemble simulations of temperature for the late 20th century period are within approximately 0.4 °C of one another (averaged across all months) for the EH region. This suggests that greater confidence can be placed in trends and changes in temperature-related projections for the EH region (as compared to the WH region). Significant negative trends in xtemp range and significant positive trends in warm nights across EH stations are associated with warming during the late 20th century. In contrast, trends observed in temperature-related indices at Gilgit station in the WH region are opposite to those observed at EH stations. As explained earlier, this is likely related to the statistically significant reductions in mean annual temperature since the 1960s reported in the Upper Indus Basin. The projections of temperature-related indices exhibit similar patterns and magnitude of change by the late 21st century across both regions. Given that the EH region has a significantly longer melt season compared to the WH region (Panday *et al.*, 2011), enhanced warming (as indicated through analyses of these indices) may further amplify the already observed glacial retreat. Furthermore, multi-model simulations of precipitation for the late 20th century period exhibit greater inter-model variability for the EH region compared to the WH region, which reduces the confidence in the projected changes in precipitation and related indices. The 21st century precipitation simulations exhibit increased mean precipitation with more frequent heavy rainfall events during monsoon season with greater inter-model variability for the EH region. In contrast, the projected changes in precipitation in the WH region are minimal and indicate a wetter cold season. In general, uncertainty is usually large in precipitation simulations and projections, particularly during monsoon because of insufficient agreement between climate models (Hawkins and Sutton, 2011; Seth *et al.*, 2011; IPCC, 2012).

5. Summary and conclusion

The results from this study provide a detailed assessment of coarse-scale, multi-model ensembles of GCM scenarios of future changes in climatic variables and extremes for the HKH region. This study examines projected changes in extremes of temperature and precipitation in the EH and WH regions within the HKH region using the CMIP3 archive under three SRES scenarios (B1, A1B, and A2) and the CMIP5 archive using RCP 8.5. Additionally, extreme climate indices of observed stations available in these regions are qualitatively compared with model simulations to investigate consistencies in the direction of trends during the 20th century. Overall, both the CMIP3 and CMIP5 models capture the 20th century mean annual cycles of temperature and precipitation in both regions well, but with a relatively large spread in capturing observational precipitation regimes. Analysis of observations shows significant negative trends for frost days at mid-elevational range (3600–3800 m) and significant increasing trends in warm nights across all EH stations. These are consistent with model-simulated temperature indices for frost days and warm nights. However, these coarse-scale models are not able to resolve fine-scale processes, and improved representation of topography is essential in projection of some indices. This is evident in results from the WH where statistically significant reductions in mean annual temperature (and therefore decreasing trends in warm nights) have been observed across stations (e.g. Gilgit) in contrast to model simulations.

Future projections of climate change under different scenarios suggest that higher elevation regions will continue to experience the strongest warming across the globe (Beniston, 2006; Bradley *et al.*, 2006; Déry, 2011; Vuille, 2011). This study indicates that the greatest increases in temperature for both the EH and WH regions occur during monsoonal months (July to September) in the A2 scenario, which coincides with the projections of increased precipitation extremes in the EH region and little change or small decreases in precipitation in the WH region. Strong modifications in either summer air temperatures or winter precipitation may affect glacier ablation and accumulation (Déry, 2011). Since glaciers in the EH region are of the summer-accumulation type, where maximum accumulation and ablation occur simultaneously during the summer (Ageta and Higuchi, 1984; Benn and Owen, 1998; Kayastha and Harrison, 2008), shifts in summer temperature and precipitation will be important overall factors in the future fate of these glaciers.

Climate model projections for regions with complex topography such as the HKH must be evaluated with caution. Higher resolution regional climate models that improve upon the topographic representation of this region are necessary to resolve finer regional scale processes and feedbacks; however, it is very important to understand how well the global models are performing before any dynamical downscaling (Tebaldi and Knutti, 2010). Additionally, the lack of long-term data from high-altitude meteorological stations makes it difficult to accurately assess and validate trends in extreme indices across the entire HKH region. The CMIP5 archive includes more comprehensive models with overall finer spatial resolution compared with CMIP3 (Taylor *et al.*, 2012), although they appear to have a greater model spread than CMIP3 models particularly in simulating temperatures in the HKH region. In this study, annual cycle projections for precipitation and temperature indicate better agreement among models for the middle 21st century projections compared to the late 21st century projections based on a subset of the CMIP3 model outputs. The observed and projected shifts in extreme indices in this region demands further understanding and examination of the climatic processes and trends to avoid potential negative impacts to water resources. Our study provides a baseline for assessing trends in temperature, precipitation, and extreme indices, presenting a first step towards constituting critical information needed for climate impacts assessment across the HKH region.

Acknowledgements

This research was funded in part by a NASA Earth Science Fellowship (Grant No. NNX10AO65H). J. Thibeault's effort was supported in part by NSF CAREER Award #1056216. We acknowledge the World Climate Research Programme's Working Group on Coupled Modelling, which is responsible for CMIP3 and CMIP5 archives, and we thank the climate modelling groups for producing and making available their model output. For CMIP, the U.S. Department of Energy's Program for Climate Model Diagnosis and Intercomparison provides coordinating support and led development of software infrastructure in partnership with the Global Organization for Earth System Science Portals. We acknowledge the CLIMDEX project maintained by the researchers at the Climate Change Research Centre, The University of New South Wales, for providing the CMIP5 model indices and runs, and the HadEX2 data set.

Supporting Information

The following supporting information is available as part of the online article:

Figure S1. Multi-model average (CMIP5) for late 20th century historical simulations (1970–1999) for temperature (°C) and precipitation (mm day^{-1}) compared with CRU gridded observations for the EH and WH regions. Modern counterparts to the CMIP3 models used in this study, i.e. CCSM4, CNRM-CM5, GFDL-ESM2G, IPSL-CM5A-LR, MIROC-ESM, MIROC5, and MRI-CGCM3.

Figure S2. Change in distributions for multi-model average historical and RCP 8.5 stimulated (a) frost days, and (b) cumulative dry days. Three periods are shown: 1970–1999 (black), 2020–2049 (red), and 2070–2099 (dashed red). HadEX2 (blue) observations for the 1970–1999 period are shown for comparison.

Figure S3. Box plots show CMIP3 multi-model statistics for standardized monthly temperature (a–c) and precipitation (d–f) differences for the EH region (mid-21st century minus 1970–1999) for SRES B1, A1B, and A2. The interquartile range (IQR) is shaded and horizontal black lines represent multi-model median values. Multi-model averages are represented by black circles. The whiskers represent the furthest model value within 1.5 times the IQR. Open circles represent outliers.

Figure S4. Multi-model average (CMIP5) for late 20th century historical simulations (1970–1999) for standardized temperature and precipitation differences (mid-21st century minus 1970–1999) for the WH region. Modern counterparts to the CMIP3 models used in this study, i.e. CCSM4, CNRM-CM5, GFDL-ESM2G, IPSL-CM5A-LR, MIROC-ESM, MIROC5, and MRI-CGCM3.

Figure S5. Box plots show CMIP5 multi-model statistics for mid-21st century standardized monthly temperature and precipitation differences (late 21st century minus 1970–1999) for the EH region (a and c) and WH region (b and d) for RCP 8.5. The interquartile range (IQR) is shaded and horizontal black lines represent multi-model median values. Multi-model averages are represented by black circles. The whiskers represent the furthest model value within 1.5 times the IQR. Open circles represent outliers. Modern counterparts to the CMIP3 models used in this study, i.e. CCSM4, CNRM-CM5, GFDL-ESM2G, IPSL-CM5A-LR, MIROC-ESM, MIROC5, and MRI-CGCM3.

Table S1. CMIP3 coupled ocean-atmosphere models used in this study. Atmospheric resolution is shown in longitude by latitude degrees, whereas ocean resolution is defined as the number of grids in longitude and latitude.

Table S2. CMIP5 models used in this analysis.

Table S3. Extreme indices used in this study and their definitions, adapted from Alexander *et al.* (2006) and Sillmann *et al.* (2013a, 2013b).

References

Adam JC, Hamlet AF, Lettenmaier DP. 2009. Implications of global climate change for snowmelt hydrology in the twenty-first century. *Hydrol. Processes* **23**: 962–972, doi: 10.1002/hyp.7201.

Ageta Y, Higuchi K. 1984. Estimation of mass balance components of a summer-accumulation type glacier in the Nepal Himalaya. *Geogr. Ann. A Phys. Geogr.* **66**: 249–255, doi: 10.2307/520698.

Alexander LV, Zhang X, Peterson TC, Caesar J, Gleason B, Tank AMGK, Haylock M, Collins D, Trewin B, Rahimzadeh F, Tagipour A, Kumar KR, Revadekar J, Griffiths G, Vincent L, Stephenson DB, Burn J, Aguilar E, Brunet M, Taylor M, New M, Zhai P, Rusticucci M, Vazquez-Aguirre JL. 2006. Global observed changes in daily climate extremes of temperature and precipitation. *J. Geophys. Res.* **111**: D05109, doi: 10.1029/2005JD006290.

Beniston M. 2006. Mountain weather and climate: a general overview and a focus on climatic change in the Alps. *Hydrobiologia* **562**: 3–16, doi: 10.1007/s10750-005-1802-0.

Benn DI, Owen LA. 1998. The role of the Indian summer monsoon and the mid-latitude westerlies in Himalayan glaciation: review and speculative discussion. *J. Geol. Soc.* **155**: 353–363, doi: 10.1144/gsjgs.155.2.0353.

Bolch T, Kulkarni A, Kääb A, Huggel C, Paul F, Cogley J, Frey H, Kargel J, Fujita K, Scheel M. 2012. The state and fate of Himalayan glaciers. *Science* **336**: 310–314, doi: 10.1126/science.1215828.

Bradley RS, Vuille M, Diaz HF, Vergara W. 2006. Threats to water supplies in the tropical Andes. *Science* **312**: 1755, doi: 10.1126/science.1128087.

Chalise S. 1994. Mountain environments and climate change in the Hindu Kush-Himalayas. In *Mountain Environments in Changing Climates*, Beniston M (ed). Routledge: London, 308–324.

Chaturvedi RK, Kulkarni A, Karyakarte Y, Joshi J, Bala G. 2014. Glacial mass balance changes in the Karakoram and Himalaya based on CMIP5 multi-model climate projections. *Clim. Change* **123**: 315–328.

Coppola E, Giorgi F. 2010. An assessment of temperature and precipitation change projections over Italy from recent global and regional climate model simulations. *Int. J. Climatol.* **30**: 11–32, doi: 10.1002/joc.1867.

Coumou D, Rahmstorf S. 2012. A decade of weather extremes. *Nat. Clim. Change* **2**: 491–496, doi: 10.1038/nclimate1452.

Déry SJ. 2011. Global warming and its effect on snow/ice/glaciers. In *Encyclopedia of Snow, Ice and Glaciers*, Singh VP, Singh P, Haritashya (eds). Springer Verlag: Dordrecht, Netherlands, 468–471.

Donat M, Alexander L, Yang H, Durre I, Vose R, Dunn R, Willett K, Aguilar E, Brunet M, Caesar J. 2013. Updated analyses of temperature and precipitation extreme indices since the beginning of the twentieth century: the HadEX2 dataset. *J. Geophys. Res. Atmos* **118**(5): 2098–2118.

Douville H, Royer JF, Polcher J, Cox P, Gedney N, Stephenson DB, Valdes PJ. 2000. Impact of CO_2 doubling on the Asian summer monsoon: robust versus model-dependent responses. *J. Meteorol. Soc. Jpn.* **78**: 421–439.

Easterling DR, Meehl GA, Parmesan C, Changnon SA, Karl TR, Mearns LO. 2000. Climate extremes: observations, modeling, and impacts. *Science* **289**: 2068–2074, doi: 10.1126/science.289.5487.2068.

Fan F, Mann ME, Lee S, Evans JL. 2010. Observed and modeled changes in the South Asian summer monsoon over the historical period. *J. Clim.* **23**: 5193–5205, doi: 10.1175/2010jcli3374.1.

Fowler HJ, Archer DR. 2006. Conflicting signals of climatic change in the Upper Indus Basin. *J. Clim.* **19**: 4276–4293, doi: 10.1175/jcli3860.1.

Frich P, Alexander L, Della-Marta P, Gleason B, Haylock M, Klein Tank A, Peterson T. 2002. Observed coherent changes in climatic extremes during the second half of the twentieth century. *Clim. Res.* **19**: 193–212, doi: 10.3354/cr019193.

Gardelle J, Berthier E, Arnaud Y. 2012. Slight mass gain of Karakoram glaciers in the early twenty-first century. *Nat. Geosci.* **5**: 322–325, doi: 10.1038/ngeo1450.

Gautam R, Hsu NC, Lau KM. 2010. Pre-monsoon aerosol characterization and radiative effects over the Indo-Gangetic plains: implications for regional climate warming. *J. Geophys. Res.* **115**: D17208, doi: 10.1029/2010jd013819.

Hawkins E, Sutton R. 2009. The potential to narrow uncertainty in regional climate predictions. *Bull. Am. Meteorol. Soc.* **90**: 1095–1107.

Hawkins E, Sutton R. 2011. The potential to narrow uncertainty in projections of regional precipitation change. *Clim. Dyn.* **37**: 407–418, doi: 10.1007/s00382-010-0810-6.

Hipel KW, McLeod AI. 1994. *Time Series Modelling of Water Resources and Environmental Systems*. Elsevier Science: Amsterdam, The Netherlands.

Huggel C, Salzmann N, Allen S, Caplan-Auerbach J, Fischer L, Haeberli W, Larsen C, Schneider D, Wessels R. 2010. Recent and future warm extreme events and high-mountain slope stability. *Philos. Trans. R. Soc. A Math. Phys. Eng. Sci.* **368**: 2435–2459, doi: 10.1098/rsta.2010.0078.

IPCC. 2012. Managing the risks of extreme events and disasters to advance climate change adaptation. In *A Special Report of Working Groups I and II of the Intergovernmental Panel on Climate Change*, Field CB, Barros V, Stocker TF, Qin D, Dokken DJ, Ebi KL, Mastrandrea MD, Mach KJ, Plattner G-K, Allen SK, Tignor M, Midgley PM (eds). Cambridge University Press: Cambridge, UK, and New York, NY, 582 pp.

Kargel J, Armstrong R, Arnaud Y, Bajracharya S, Berthier E, Bishop M, Bolch T, Bush A, Cogley G, Fujita K. 2009. Satellite-era glacier changes in High Asia. In: *Background support presentation for NASA "Black Carbon and Aerosols" press conference associated with Fall AGU*, San Francisco, CA, 14 December 2009.

Kayastha RB, Harrison SP. 2008. Changes of the equilibrium-line altitude since the Little Ice Age in the Nepalese Himalaya. *Ann. Glaciol.* **48**: 93–99, doi: 10.3189/172756408784700581.

Kharin VV, Zwiers FW, Zhang X, Hegerl GC. 2007. Changes in temperature and precipitation extremes in the IPCC ensemble of global coupled model simulations. *J. Clim.* **20**: 1419–1444, doi: 10.1175/JCLI4066.1.

Klein Tank AMG, Peterson TC, Quadir DA, Dorji S, Zou X, Tang H, Santhosh K, Joshi UR, Jaswal AK, Kolli RK, Sikder AB, Deshpande NR, Revadekar JV, Yeleuova K, Vandasheva S, Faleyeva M, Gomboluudev P, Budhathoki KP, Hussain A, Afzaal M, Chandrapala L, Anvar H, Amanmurad D, Asanova VS, Jones PD, New MG, Spektorman T. 2006. Changes in daily temperature and precipitation extremes in central and south Asia. *J. Geophys. Res.* **111**: D16105, doi: 10.1029/2005JD006316.

Knutti R, Sedláček J. 2013. Robustness and uncertainties in the new CMIP5 climate model projections. *Nat. Clim. Change* **3**: 369–373.

Lau KM, Kim MK, Kim KM. 2006. Asian summer monsoon anomalies induced by aerosol direct forcing: the role of the Tibetan Plateau. *Clim. Dyn.* **26**: 855–864, doi: 10.1007/s00382-006-0114-z.

Lobell DB, Burke MB, Tebaldi C, Mastrandrea MD, Falcon WP, Naylor RL. 2008. Prioritizing climate change adaptation needs for food security in 2030. *Science* **319**: 607–610, doi: 10.1126/science.1152339.

Mann H. 1945. Nonparametric tests against trend. *Econometrica* **13**: 245–259, doi: 10.2307/1907187.

Marengo J, Jones R, Alves LM, Valverde M. 2009. Future change of temperature and precipitation extremes in South America as derived from the PRECIS regional climate modeling system. *Int. J. Climatol.* **29**: 2241–2255, doi: 10.1002/joc.1863.

Massey FJ. 1951. The Kolmogorov-Smirnov test for goodness of fit. *J. Am. Stat. Assoc.* **46**: 68–78, doi: 10.2307/2280095.

Meehl GA, Tebaldi C, Nychka D. 2004. Changes in frost days in simulations of twenty first century climate. *Clim. Dyn.* **23**: 495–511, doi: 10.1007/s00382-004-0442-9.

Meehl GA, Covey C, Delworth T, Latif M, McAvaney B, Mitchell JFB, Stouffer RJ, Taylor KE. 2007. The WCRP CMIP3 multimodel dataset. *Bull. Am. Meteorol. Soc.* **88**: 1383–1394, doi: 10.1175/BAMS-88-9-1383.

Meehl GA, Arblaster JM, Collins WD. 2008. Effects of black carbon aerosols on the Indian monsoon. *J. Clim.* **21**: 2869–2882, doi: 10.1175/2007JCLI1777.1.

Mitchell TD, Jones PD. 2005. An improved method of constructing a database of monthly climate observations and associated high-resolution grids. *Int. J. Climatol.* **25**: 693–712, doi: 10.1002/joc.1181.

Moss RH, Edmonds JA, Hibbard KA, Manning MR, Rose SK, Van Vuuren DP, Carter TR, Emori S, Kainuma M, Kram T. 2010. The next generation of scenarios for climate change research and assessment. *Nature* **463**: 747–756.

Mote P, Brekke L, Duffy PB, Maurer E. 2011. Guidelines for constructing climate scenarios. *Eos Trans. AGU* **92**: 257–258, doi: 10.1029/2011EO310001.

Nolin AW, Daly C. 2006. Mapping "at risk" snow in the Pacific Northwest. *J. Hydrometeorol.* **7**: 1164–1171, doi: 10.1175/jhm543.1.

Overpeck JT, Meehl GA, Bony S, Easterling DR. 2011. Climate data challenges in the 21st century. *Science* **331**: 700–702, doi: 10.1126/science.1197869.

Panday PK, Frey KE, Ghimire B. 2011. Detection of the timing and duration of snowmelt in the Hindu Kush-Himalaya using QuikSCAT, 2000–2008. *Environ. Res. Lett.* **6**: 1–13, doi: 10.1088/1748-9326/6/2/024007.

Peings Y, Douville H. 2010. Influence of the Eurasian snow cover on the Indian summer monsoon variability in observed climatologies and CMIP3 simulations. *Clim. Dyn.* **34**: 643–660, doi: 10.1007/s00382-009-0565-0.

Rajbhandari R, Shrestha AB, Kulkarni A, Patwardhan SK, Bajracharya SR. 2014. Projected changes in climate over the Indus river basin using a high resolution regional climate model (PRECIS). *Clim. Dyn.*, doi: 10.1007/s00382-014-2183-8.

Ren D, Karoly DJ, Leslie LM. 2007. Temperate mountain glacier-melting rates for the period 2001–30: estimates from three coupled GCM simulations for the greater Himalayas. *J. Appl. Meteorol. Climatol.* **46**: 890–899, doi: 10.1175/JAM2499.1.

Rogelj J, Meinshausen M, Knutti R. 2012. Global warming under old and new scenarios using IPCC climate sensitivity range estimates. *Nat. Clim. Change* **2**: 248–253.

Scoccimarro E, Zampieri M, Bellucci A, Navarra A. 2013. Heavy precipitation events in a warmer climate: results from CMIP5 models. *J. Clim* **26**: 7902–7911.

Sen RS. 2009. A spatial analysis of extreme hourly precipitation patterns in India. *Int. J. Climatol.* **29**: 345–355, doi: 10.1002/joc.1763.

Seth A, Rauscher SA, Rojas M, Giannini A, Camargo SJ. 2011. Enhanced spring convective barrier for monsoons in a warmer world? *Clim. Change* **104**: 403–414, doi: 10.1007/s10584-010-9973-8.

Seth A, Rauscher SA, Biasutti M, Giannini A, Camargo SJ, Rojas M. 2013. CMIP5 projected changes in the annual cycle of precipitation in monsoon regions. *J. Clim.* **26**: 7328–7351.

Shrestha AB, Devkota LP. 2010. Climate change in the Eastern Himalayas: observed trends and model directions. Climate change impact and vulnerability in the Eastern Himalayas. Technical Report 1, ICIMOD: Kathmandu.

Sillmann J, Kharin V, Zhang X, Zwiers F, Bronaugh D. 2013a. Climate extremes indices in the CMIP5 multimodel ensemble: Part 1. Model evaluation in the present climate. *J. Geophys. Res. Atmos.* **118**: 1716–1733.

Sillmann J, Kharin V, Zwiers F, Zhang X, Bronaugh D. 2013b. Climate extremes indices in the CMIP5 multimodel ensemble: Part 2. Future climate projections. *J. Geophys. Res. Atmos* **118**(6): 2473–2493.

Taylor KE, Stouffer RJ, Meehl GA. 2012. An overview of CMIP5 and the experiment design. *Bull. Am. Meteorol. Soc.* **93**(4): 485–498, doi: 10.1175/BAMS-D-11-00094.1.

Tebaldi C, Knutti R. 2010. Climate models and their projections of future changes. In *Climate Change and Food Security, Advances in Global Change Research*, Lobell D, Burke M (eds). Springer: Dordrecht, Netherlands, 31–56.

Tebaldi C, Hayhoe K, Arblaster JM, Meehl GA. 2006. Going to the extremes. *Clim. Change* **79**: 185–211, doi: 10.1007/S10584-006-9051-4.

Thibeault JM, Seth A, Garcia M. 2010. Changing climate in the Bolivian Altiplano: CMIP3 projections for temperature and precipitation extremes. *J. Geophys. Res.* **115**: D08103, doi: 10.1029/2009JD012718.

Vera C, Silvestri G. 2009. Precipitation interannual variability in South America from the WCRP-CMIP3 multi-model dataset. *Clim. Dyn.* **32**: 1003–1014, doi: 10.1007/s00382-009-0534-7.

Vuille M. 2011. Climate variability and high altitude temperature and precipitation. In *Encyclopedia of Snow, Ice and Glaciers*, Singh VP, Singh P, Haritashya (eds). Springer Verlag: Dordrecht, Netherlands, 153 pp.

Williams RS, Ferrigno JG. 2010. *Glaciers of Asia*. U.S. Geological Survey: Reston, VA, 349.

Xu J, Grumbine E, Shrestha A, Eriksson M, Yang X, Wang Y, Wilkes A. 2009. The melting Himalayas: cascading effects of climate change on water, biodiversity, and livelihoods. *Conserv. Biol.* **23**: 520–530, doi: 10.1111/j.1523-1739.2009.01237.x.

Yadav RR, Park WK, Singh J, Dubey B. 2004. Do the western Himalayas defy global warming? *Geophys. Res. Lett.* **31**: L17201, doi: 10.1029/2004GL020201.

Yang T, Hao X, Shao Q, Xu CY, Zhao C, Chen X. 2012. Multi-model ensemble projections in temperature and precipitation extremes of the Tibetan Plateau in the 21st century. *Glob. Planet. Change* **80–81**: 1–13, doi: 10.1016/j.gloplacha.2011.08.006.

Young GJ, Hewitt K. 1990. Hydrology research in the upper Indus basin, Karakoram Himalaya, Pakistan. In *Hydrology of Mountainous Areas*, Molñar L (ed). IASH: Czechoslovakia, Europe, 139–152.